

A Chemically Stable Hofmann-Type Metal–Organic Framework with Sandwich-Like Binding Sites for Benchmark Acetylene Capture

Jiyan Pei, Kai Shao, Jia-Xin Wang, Hui-Min Wen, Yu Yang, Yuanjing Cui, Rajamani Krishna, Bin Li,* and Guodong Qian*

The realization of porous materials for highly selective separation of acetylene (C_2H_2) from various other gases (e.g., carbon dioxide and ethylene) by adsorption is of prime importance but challenging in the petrochemical industry. Herein, a chemically stable Hofmann-type metal–organic framework (MOF), $Co(py_2z)[Ni(CN)_4]$ (termed as ZJU-74a), that features sandwich-like binding sites for benchmark C_2H_2 capture and separation is reported. Gas sorption isotherms reveal that ZJU-74a exhibits by far the record C_2H_2 capture capacity ($49\text{ cm}^3\text{ g}^{-1}$ at 0.01 bar and 296 K) and thus ultrahigh selectivity for C_2H_2/CO_2 (36.5), C_2H_2/C_2H_4 (24.2), and C_2H_2/CH_4 (1312.9) separation at ambient conditions, respectively, of which the C_2H_2/CO_2 selectivity is the highest among all the robust MOFs reported so far. Theoretical calculations indicate that the oppositely adjacent nickel(II) centers together with cyanide groups from different layers in ZJU-74a can construct a sandwich-type adsorption site to offer dually strong and cooperative interactions for the C_2H_2 molecule, thus leading to its ultrahigh C_2H_2 capture capacity and selectivities. The exceptional separation performance of ZJU-74a is confirmed by both simulated and experimental breakthrough curves for 50/50 (v/v) C_2H_2/CO_2 , 1/99 C_2H_2/C_2H_4 , and 50/50 C_2H_2/CH_4 mixtures under ambient conditions.

Acetylene (C_2H_2) is an important industrial gas that has been widely used as fuels in welding/cutting or as feedstocks for the production of commercial chemicals such as vinyl chloride, acrylic acid, and 1,4-butyne diol.^[1,2] C_2H_2 is typically generated

by the combustion of natural gas or the cracking of hydrocarbons, inevitably coexisting with some of carbon dioxide (CO_2) or unconverted methane (CH_4).^[3] Purification of C_2H_2 from CO_2 or CH_4 is of industrial importance to obtain high-purity C_2H_2 for the manufacture of relative chemicals. Further, C_2H_2 is unstable and highly reactive that may induce some undesirable reactions in various industrial processes.^[4] For instance, a trace amount of C_2H_2 acts as a catalyst poison during ethylene (C_2H_4) polymerization processes, which needs to be removed to an acceptable level of no more than 40 ppm. Therefore, acetylene capture and separation is of industrial relevance to two different points of view: the removal of trace C_2H_2 impurities from ethylene, and the purification of C_2H_2 from contaminants for its pure form. Compared with traditional solvent extraction or cryogenic distillation,^[5,6] adsorptive separation based on porous materials is more environmentally

friendly and energy-efficient for separation of C_2H_2 from other gases. In this context, realization of C_2H_2 -selective adsorbents with strong C_2H_2 capture capacity is highly desirable to target high performance for all these gas separations.


Metal–organic frameworks (MOFs) or porous coordination polymers have emerged as promising adsorbents for gas separation and purification owing to their powerful predictability and tunability on pore size/shape and functionality.^[7–9] Since C_2H_2 (kinetic diameter: 3.3 Å) has a relatively large size or polarity difference with C_2H_4 (4.2 Å) and CH_4 (3.8 Å), highly efficient separation of C_2H_2/C_2H_4 or C_2H_2/CH_4 has been fulfilled in some reported MOFs with benchmark selectivities by pore tuning and pore functionalization strategies.^[10,11] However, compared with the separation of C_2H_2/C_2H_4 and C_2H_2/CH_4 , C_2H_2/CO_2 separation is much more difficult and challenging because of their very close molecular size/shape (3.3 Å for both C_2H_2 and CO_2) and physical properties.^[12] Fine tuning of pore size or flexibility on MOFs is quite limited to achieve high separation performance for C_2H_2/CO_2 separation.^[13] In this context, the most popular strategy is to immobilize functional groups/sites onto the pores to enforce the binding affinity with C_2H_2 and thus enhance C_2H_2/CO_2 selectivity.^[14–20]

J. Pei, K. Shao, J.-X. Wang, Dr. Y. Yang, Prof. Y. Cui, Prof. B. Li, Prof. G. Qian

State Key Laboratory of Silicon Materials
Cyrus Tang Center for Sensor Materials and Applications
Department of Materials Science and Engineering
Zhejiang University
Hangzhou 310027, China
E-mail: bin.li@zju.edu.cn; gdqian@zju.edu.cn

Dr. H.-M. Wen
College of Chemical Engineering
Zhejiang University of Technology
Zhejiang 310014, China

Prof. R. Krishna
Van't Hoff Institute for Molecular Sciences
University of Amsterdam
Science Park 904, Amsterdam 1098 XH, Netherlands

 The ORCID identification number(s) for the author(s) of this article can be found under <https://doi.org/10.1002/adma.201908275>.

DOI: 10.1002/adma.201908275

The well-established cases of MOFs are those with open metal sites (OMSs) that can bind acetylene significantly. For example, MOF-74 series shows high density of OMSs that have strong interactions with C_2H_2 , leading to their high C_2H_2 uptakes and moderate C_2H_2/CO_2 selectivities.^[17,18] The isomer UTSA-74 has a higher volumetric density of OMSs ($8.25 \text{ mmol cm}^{-3}$) than MOF-74 ($7.50 \text{ mmol cm}^{-3}$), thus exhibiting an enhanced C_2H_2/CO_2 selectivity.^[19] Further increase on the C_2H_2 affinity in NKMOF-1-Ni with OMSs and additional binding sites affords the benchmark C_2H_2/CO_2 selectivity of 22 at ambient conditions.^[20] Evidently, the design of porous materials with strong binding affinity for C_2H_2 provides a promising strategy to address industrial challenges related to C_2H_2 separation, especially for C_2H_2/CO_2 separation.

Current MOFs with OMSs typically allow one adsorbed C_2H_2 molecule to interact with one metal site due to inadequate overlap of potential fields between two metal sites. Such single metal- C_2H_2 interaction would delimit the acetylene binding strength and thus the capture capacity at low-pressure region in most cases, as exemplified by HKUST-1,^[17b] Zn-MOF-74,^[17a] and UTSA-74.^[19] To achieve stronger C_2H_2 binding within a MOF, we speculated that if two opposite coordinatively unsaturated metal centers are adjacent with a suitable distance, a sandwich-like binding model for C_2H_2 can be generated based on the dual and cooperative interactions between C_2H_2 molecule and the two metal sites, thus probably affording ultrahigh C_2H_2 binding affinity and capture capacity. With this in mind, we herein realized a chemically stable Hofmann-type ultramicroporous MOF, $Co(pyz)[Ni(CN)_4]$ (ZJU-74, *pyz* = pyrazine) that features oppositely adjacent open metal ions and densely populated cyanide groups thus providing a sandwich-like binding environment to capture C_2H_2 molecules (Figure 1). Our experimental and simulation studies verify this hypothesis, and the activated ZJU-74a shows the benchmark C_2H_2 affinity

and thus the highest C_2H_2 adsorption capacity of $49 \text{ cm}^3 \text{ g}^{-1}$ at 0.01 bar and 296 K, as well as very high C_2H_2/CO_2 , C_2H_2/C_2H_4 and C_2H_2/CH_4 selectivities under such conditions.

Complete structures for ZJU-74 have not been determined, and the likely model was simulated based on powder diffraction data in the previous literatures reported.^[21] To get the accurate structure information, orange square-block-shaped crystals of ZJU-74 suitable for X-ray analysis were prepared by slow diffusion of a methanol/water solution of $Co(NO_3)_2 \cdot 6H_2O$ and *pyz* into a $K_2[Ni(CN)_4] \cdot nH_2O$ solution for 2 weeks. The single-crystal X-ray diffraction analysis revealed that ZJU-74 adopts a 3D network that crystallizes in a tetragonal $P4/mmm$ space group. As shown in Figure 1a, four terminal nitrogen atoms of the $[Ni(CN)_4]^{2-}$ anion units are coordinated to cobalt(II) atoms to generate a 2D square grid-like $\{Co[Ni(CN)_4]\}_n$ layers. The 2D layers are pillared by the *pyz* ligands to form a 3D network without interpenetration. Thus, each Co^{2+} site shows six coordinated octahedral geometry, completed by six nitrogen atoms originated from four $[Ni(CN)_4]^{2-}$ anions and two *pyz* ligands. Topologically, ZJU-74 possesses a 4,6-connected *psc*-net. This network yields channels with dimensions of about $3.8 \times 3.6 \text{ \AA}^2$ along the *a* or *b* axis. Due to the planarity of $[Ni(CN)_4]^{2-}$ units, each Ni(II) site shows two accessible binding sites perpendicular to the layer plane. The calculated density of open Ni(II) sites can reach $9.05 \text{ mmol cm}^{-3}$, which is even higher than the well-known MOF-74 ($7.50 \text{ mmol cm}^{-3}$) and UTSA-74 ($8.25 \text{ mmol cm}^{-3}$). In addition, due to the small pore size of ZJU-74, the Ni-Ni distance from adjacent layers are only 3.6 \AA after subtracting the van der Waals radius, which is very suitable to trap a C_2H_2 molecule (3.3 \AA). As a result, these adjacent two $[Ni(CN)_4]^{2-}$ building units along with a suitable pore size can form a sandwich-like binding environment to efficiently capture C_2H_2 molecule (Figure 1b), endowing ZJU-74 with the potentially ultrahigh C_2H_2 affinity and capture capacity.

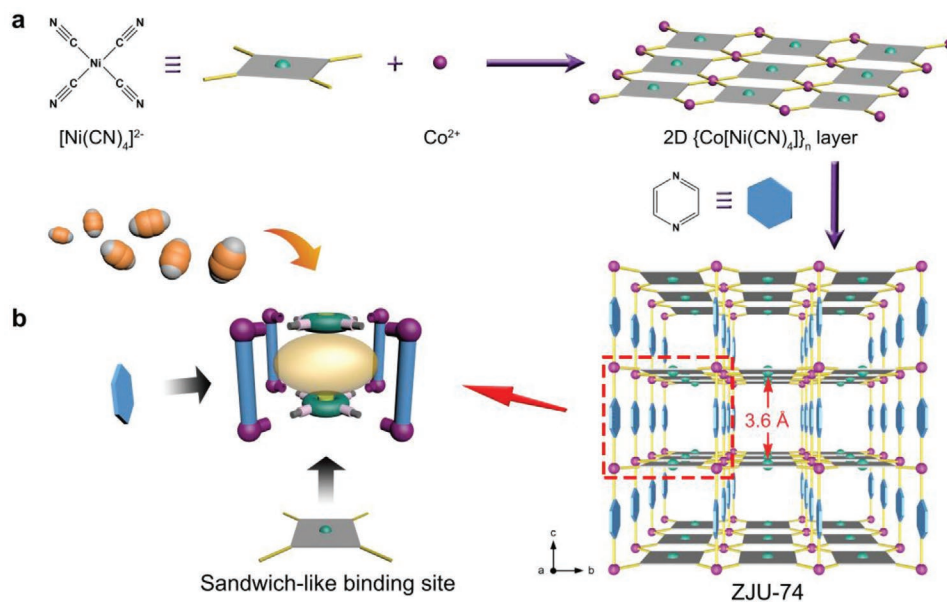


Figure 1. Structure description of ZJU-74. a) Construction of $2D \{Co[Ni(CN)_4]\}_n$ layers with *pyz* ligands to form 3D Hofmann-type networks in ZJU-74. b) Schematic illustration of the sandwich-like binding site in ZJU-74 for C_2H_2 capture. The Co^{2+} ion is shown in purple sphere, the *pyz* ligand is shown in blue pillar, and the open metal site is shown in green and yellow column; orange ellipsoid represents the cavity for C_2H_2 adsorption.

The permanent porosity of the activated ZJU-74a was confirmed by nitrogen (N_2) adsorption isotherms at 77 K. As shown in Figure S3, Supporting Information, ZJU-74a takes up a $200.7 \text{ cm}^3 \text{ g}^{-1}$ amount of N_2 at 77 K and 1 bar, and the nitrogen isotherm shows a significant type I sorption behavior without any hysteresis, characteristic of microporous materials. The Brunauer–Emmett–Teller surface area was calculated to be $694 \text{ m}^2 \text{ g}^{-1}$. The pore size distribution is shown in Figure S4, Supporting Information, determined by Horvath-Kawazoe method based on 77 K N_2 isotherms. The calculated pore size (3.9 \AA) is in good agreement with the value (3.6 \AA) obtained from the crystal structure.

Pure component equilibrium adsorption isotherms of C_2H_2 , CO_2 , C_2H_4 , and CH_4 were measured at different temperatures up to 1 bar (Figures S5–S8, Supporting Information), respectively. As shown in Figure 2a, ZJU-74a shows extremely steep variable temperature adsorption isotherms at very low pressure, and almost saturation ($\sim 76 \text{ cm}^3 \text{ g}^{-1}$) at around 0.1 bar and 296 K. The total C_2H_2 uptake at 296 K and 1 bar can reach $85.7 \text{ cm}^3 \text{ g}^{-1}$. This C_2H_2 uptake at 0.1 bar approaches the stoichiometric quantity (3.35 mmol g^{-1} or $75 \text{ cm}^3 \text{ g}^{-1}$) expected if one gas molecule is adsorbed per Ni(II) site, indicating that the Ni(II) sites mainly account for its low-pressure C_2H_2 uptake. Due to the record-high density of OMSs and sandwich-like adsorption sites between two $[Ni(CN)_4]^{2-}$ units, ZJU-74a exhibits the ultra-strong affinity toward C_2H_2 molecule, resulting in an exceptionally high gravimetric C_2H_2 uptake of $49.0 \text{ cm}^3 \text{ g}^{-1}$ at 0.01 bar and 296 K. As shown in Figure 2c and Table S1,

Supporting Information, this C_2H_2 uptake is higher than all the MOFs reported including the previous benchmark NKMOF-1-Ni^[20] ($39 \text{ cm}^3 \text{ g}^{-1}$) and UTSA-200a^[10c] ($41 \text{ cm}^3 \text{ g}^{-1}$), setting a new benchmark for C_2H_2 capture uptake at 0.01 bar. On the contrary, ZJU-74a shows significantly low C_2H_4 , CO_2 , and CH_4 uptakes at low pressure regions (Figure 2b). These adsorption differences between these gases were also confirmed by the isosteric heat of adsorption (Q_{st}), calculated by adsorption isotherms at different temperatures. As shown in Figure 2d, the Q_{st} values of C_2H_2 are in the range of $45\text{--}65 \text{ kJ mol}^{-1}$, which is notably higher than that of C_2H_4 , CO_2 , and CH_4 in the whole range. The maximum Q_{st} value of C_2H_2 for ZJU-74a is even higher than those MOFs with high density of OMSs, such as NKMOF-1-Ni (60.3 kJ mol^{-1}),^[20] Zn-MOF-74 (31.7 kJ mol^{-1}),^[19] and UTSA-74a (33 kJ mol^{-1}),^[19] further confirming its benchmark C_2H_2 affinity and capture capacity. The time-dependent desorption kinetics studies of ZJU-74a showed that the adsorbed C_2H_2 and CO_2 can be completely removed under a high vacuum for ca. 36 and 16 min at 296 K (Figure S14, Supporting Information), respectively.

The adsorption selectivities of ZJU-74a for 50/50 C_2H_2/CO_2 , 1/99 C_2H_2/C_2H_4 , and 50/50 C_2H_2/CH_4 mixtures were predicted by using ideal adsorbed solution theory (IAST), respectively. Figure 2e shows the data obtained at 296 K. Due to the benchmark C_2H_2 capture capacity at low pressure, ZJU-74a exhibits an ultrahigh C_2H_2/CO_2 selectivity up to 170 at 0.01 bar and 296 K. With the increase of pressure, it gradually decreases down to 36.5 at 1 bar. It is worth to note that this C_2H_2/CO_2

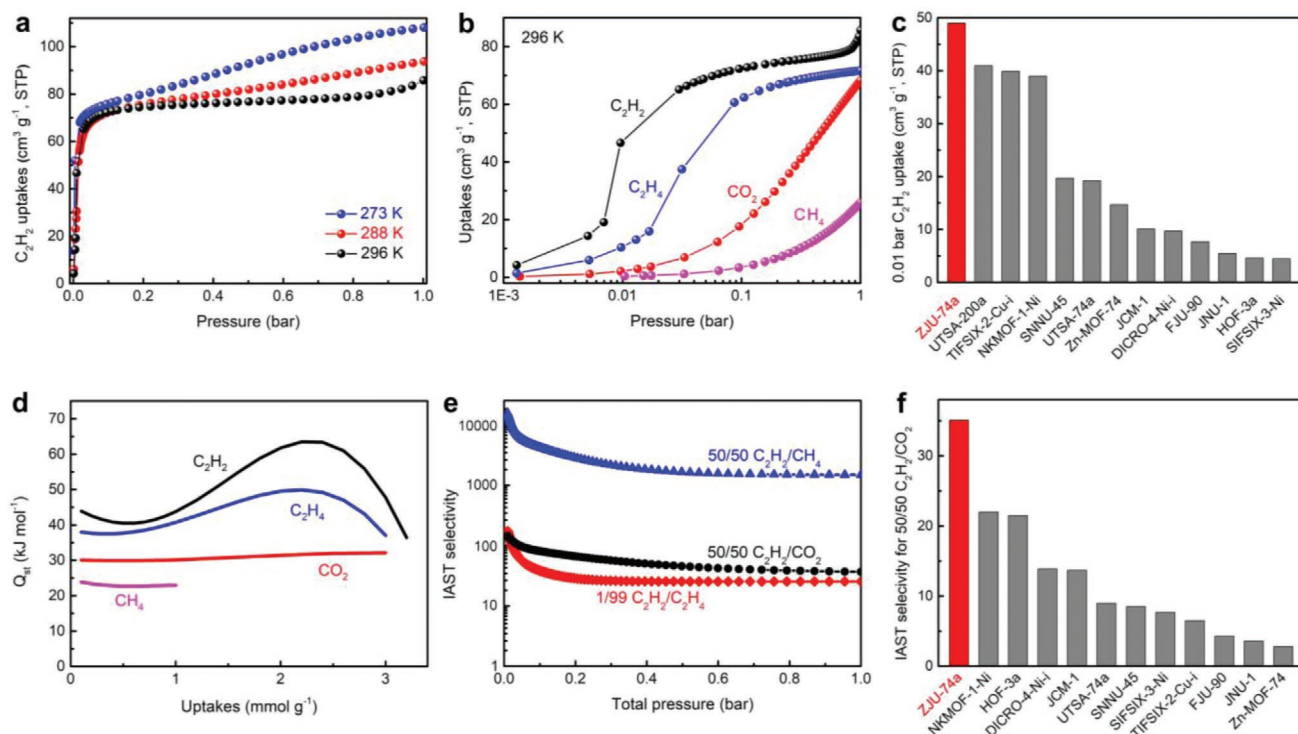


Figure 2. a) C_2H_2 adsorption isotherms of ZJU-74a at different temperatures. b) Gas adsorption isotherms of ZJU-74a for C_2H_2 (black), C_2H_4 (blue), CO_2 (red), and CH_4 (magenta) at 296 K. c) Comparison of C_2H_2 capture capacity for ZJU-74a and other best-performing materials at 0.01 bar and room temperature. d) Heats of adsorption (Q_{st}) of C_2H_2 (black), C_2H_4 (blue), CO_2 (red), and CH_4 (magenta) for ZJU-74a. e) IAST selectivities of ZJU-74a for C_2H_2/CH_4 (blue), C_2H_2/CO_2 (black), and C_2H_2/C_2H_4 (red) mixtures at 296 K. f) Comparison of the 50/50 C_2H_2/CO_2 selectivity for ZJU-74a with other best-performing rigid materials.

selectivity is the highest reported so far among all the robust MOFs at ambient conditions (Figure 2f and Figure S15, Supporting Information), notably higher than the previous best-performing materials such as NKMOF-1-Ni (22),^[20] HOF-3a (21),^[22] JCM-1 (13.7),^[15a] and UTSA-74a (9).^[19] Similarly, ZJU-74a also exhibits an ultrahigh selectivity of over 15000 and 173.5 for 50/50 C₂H₂/CH₄ and 1/99 C₂H₂/C₂H₄ mixtures at 0.01 bar and 296 K, respectively, which can be maintained to 1312.9 and 24.2 at 1 bar for these two mixtures. These benchmark gas selectivities render ZJU-74a among the best-performing materials reported for C₂H₂ capture from some industrially relevant C₂H₂ separation applications.

To gain better insight into the benchmark C₂H₂ capture capacity and selectivity of ZJU-74a, grand canonical Monte Carlo simulations were performed to investigate the interactions between ZJU-74a and various gas molecules. The calculated binding sites of C₂H₂ and CO₂ are shown in Figure 3a,b. The C₂H₂ molecules are preferentially located at the middle of two open nickel(II) sites within the square-shaped channels of ZJU-74a, displaying a side-on binding mode. The C≡C bond of each C₂H₂ molecule interacts with two Ni²⁺ ions with a distance of 3.554 Å, which are comparable with the sum of the vdW radii of carbon (1.70 Å) and nickel (1.63 Å) atoms. This distance is even notably shorter than that found in Co-MOF-74 (≈4.0 Å),^[17a] indicating a stronger interactions between C₂H₂ and metal ions in ZJU-74a. Additionally, two hydrogen atoms of each C₂H₂ molecule are also bound by eight nitrogen atoms from two different [Ni(CN)₄]²⁻ anions through cooperative C–H⋯N H-bonding with a distance of 4.173 Å. Evidently, two [Ni(CN)₄]²⁻ building units from adjacent layers can construct a sandwich-like binding environment to dually and strongly interact

with C₂H₂, thus affording its benchmark affinity and capture capacity for C₂H₂. The similar side-on binding mode was also observed on C₂H₄ molecule (Figure S17, Supporting Information). Unlike C₂H₂ molecule, the CO₂ molecule is located at the middle of two open nickel(II) sites, but interact with Ni²⁺ ions through Ni⋯O=C=O with end-on configuration (≈2.935 Å). This binding model without the sandwich-like multi-binding sites enables it to show a weaker interaction with the MOF. The calculated binding energy for C₂H₂ and CO₂ is 38 kJ mol⁻¹ and 23 kJ mol⁻¹, respectively, which are consistent well with the higher experimental Q_{st} value of C₂H₂ than that of CO₂ (Figure 2d). In addition, we note that a full occupancy of these OMSs would correspond to 3.35 mmol g⁻¹ gas uptake, which is very close to the experimental C₂H₂ uptake (3.39 mmol g⁻¹) at 296 K and 0.1 bar. These calculation results are fully consistent with our experimental findings, which can explain the benchmark C₂H₂ adsorption and separation behaviors at low pressure qualitatively.

Transient breakthrough simulations were performed to validate the feasibility of using ZJU-74a in a fixed bed for the separation of 50/50 C₂H₂/CO₂, 1/99 C₂H₂/C₂H₄, and 50/50 C₂H₂/CH₄ mixtures, respectively. Figure 3c reveals the molar concentrations of C₂H₂/CO₂, C₂H₂/C₂H₄, or C₂H₂/CH₄ exiting the adsorber packed with ZJU-74a as a function of the dimensionless time, τ, at 1 bar and 298 K, respectively. Efficient separation can be accomplished by ZJU-74a for all the gas mixtures, whereby CO₂, C₂H₄, or CH₄ gas breakthrough occurred first for C₂H₂/CO₂, C₂H₂/C₂H₄ or C₂H₂/CH₄ separation, respectively, and then C₂H₂ passed through the fixed bed after a certain time (τ_{break}) because C₂H₂ is more efficiently captured by the ZJU-74a bed.

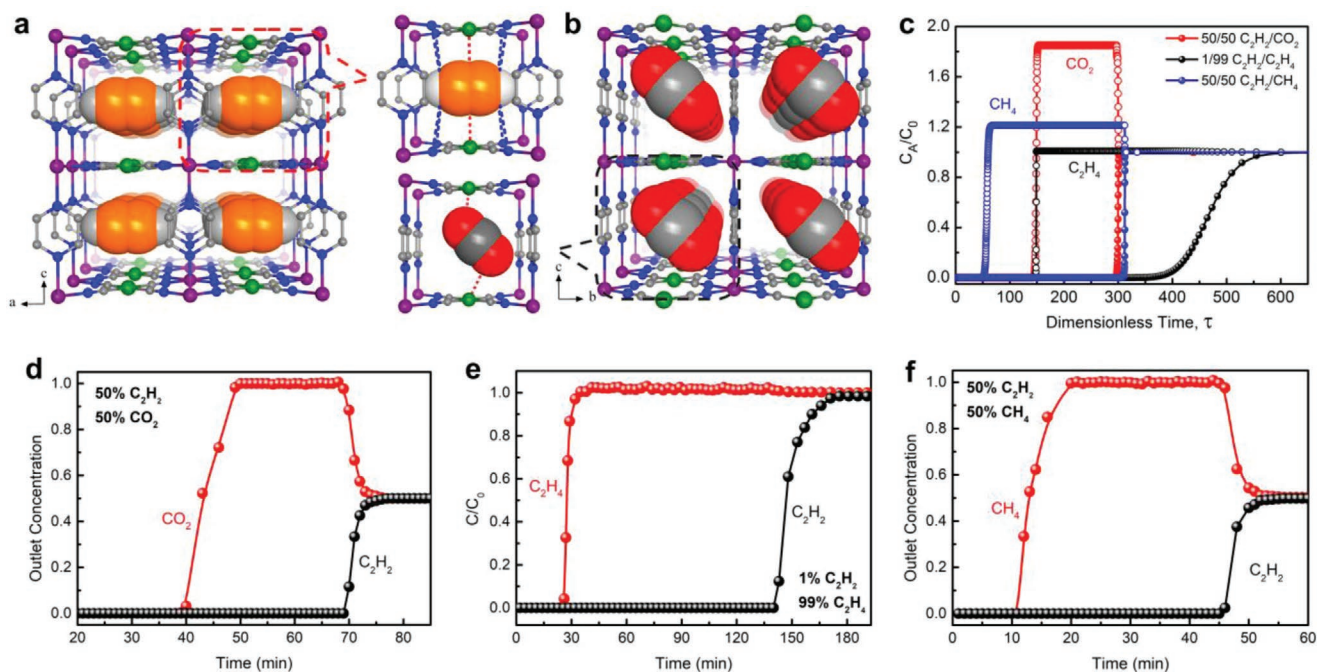


Figure 3. a) Comparison of the C₂H₂ and b) CO₂ molecule binding sites in ZJU-74a by theoretical calculations. Color code: Ni (green), Co (purple), N (blue), and C (gray). c) Simulated column breakthrough curves of ZJU-74a for 50/50 C₂H₂/CO₂, 1/99 C₂H₂/C₂H₄, and 50/50 C₂H₂/CH₄ separation, respectively. d) Experimental column breakthrough curves for a 50/50 C₂H₂/CO₂ mixture, e) a 1/99 C₂H₂/C₂H₄ mixture and f) a 50/50 C₂H₂/CH₄ mixture with a total flow of 2 mL min⁻¹ in an adsorber bed packed with ZJU-74a at 298 K and 1 bar.

Next, experimental breakthrough studies were performed in a packed column of activated ZJU-74a to evaluate its separation performance for actual 50/50 C_2H_2/CO_2 (dry and wet), 1/99 C_2H_2/C_2H_4 , and 50/50 C_2H_2/CH_4 mixtures at room temperature under a total flow of 2 mL min^{-1} , respectively. As shown in Figure 3d, it was clear that ZJU-74a can effectively separate dry C_2H_2/CO_2 gas mixture, wherein CO_2 gas first eluted through the adsorption bed, while C_2H_2 breakthrough did not occur until 68 min. During this breakthrough process, the captured C_2H_2 amount for a given cycle was calculated to be 3.64 mmol g^{-1} , 95% of the saturated uptake (3.83 mmol g^{-1}) from the single-component gas isotherms at ambient conditions. According to the breakthrough curves, the selectivity of ZJU-74a for dry C_2H_2/CO_2 mixture was calculated up to 4.3, higher than that of the benchmark NKMOF-1-Ni (2.6),^[20] SNNU-45 (2.9),^[13b] HOF-3a (2.0),^[22] and FJU-22a (1.9).^[15c] To investigate the influence of moisture, we conducted the breakthrough experiments on a wet C_2H_2/CO_2 (50/50) mixture with 60% humidity. As shown in Figure S18 and Table S5, Supporting Information, ZJU-74a can mostly retain its exceptional separation performance with the selectivity of 4.1 and 88% C_2H_2 uptake capacity (dry), in which the small decrease may arise from small amount of OMSs occupied by water molecules. In addition, after exposure to an air environment with 50–70% humidity for 2 months, the re-activated material still possesses nearly the same separation performance for dry C_2H_2/CO_2 mixture (Figure S19, Supporting Information). These results indicate that moisture only has a little effect on the separation capacity of ZJU-74a. After the breakthrough experiments, the material can be readily regenerated under a He flow (10 mL min^{-1}) at 373 K. As depicted in Figure S20, Supporting Information, the adsorbed C_2H_2 gas can be completely recovered with high purity and no detectable C_2H_2 and CO_2 were found at the outlet after 26 min.

For 1/99 C_2H_2/C_2H_4 and 50/50 C_2H_2/CH_4 mixtures (Figure 3e,f), C_2H_4 and CH_4 passed through the adsorption bed firstly, and C_2H_2 breakthrough occurred at 140 min and 45 min, respectively. Detailed gas chromatography data revealed that the concentration of C_2H_2 in the outlet effluent is less than 5 ppm before breakthrough, affording high purity of C_2H_4 and CH_4 up to 99.9995%. During the breakthrough processes, the pure C_2H_4 and CH_4 production from the outlet effluent for a given cycle were analyzed to be 12.22 and 3.21 mmol g^{-1} , respectively. These breakthrough results reveal that ZJU-74a preferentially adsorbs C_2H_2 in all the tested gas separations due to its benchmark C_2H_2 capture capacity, thus resulting in the exceptional performance for all these gas separations. Multiple C_2H_2/CO_2 (50/50) mixed-gas column breakthrough tests indicate that the separation performance of ZJU-74a can be recycled at least five continuous cycles (Figure S21, Supporting Information), confirming its good recyclability for gas separation. As inferred from the powder X-ray diffraction (PXRD) and gas adsorption experiments on associated samples, ZJU-74a remains its structural integrity after multiple adsorption tests and various breakthrough experiments (Figures S22–S24, Supporting Information).

The C_2H_2 -relevant separation tasks are typically implemented under more extreme conditions in real-world applications. For example, in the cases of C_2H_2/CO_2 and C_2H_2/CH_4 separation, the C_2H_2 raw streams, produced from the combustion of

natural gas or the cracking of hydrocarbons, typically contain a small amount of water and acidic gases.^[23] In the production of high-purity C_2H_4 , the feed gases for C_2H_2 removal are also contaminated with trace levels of water.^[24] These extreme separation conditions require adsorbents with extremely high and long-term water and pH stabilities. We thus investigated the chemical stability of ZJU-74 toward water and acid-base environments. We exposed ZJU-74 samples to different chemical environments for 3 days, including water, boiling water, aqueous solutions of pH between 1 and 12, 6 M HCl and 18 M H_2SO_4 . As shown in Figure 4a, Figures S25 and S26, Supporting Information, the framework of ZJU-74 is stable in these conditions for several days, and no loss in crystallinity and no phase change were observed by PXRD. Moreover, N_2 adsorption isotherms at 77 K and C_2H_2 uptake capacity at 296 K after treatment are very close to those of as-synthesized materials, further confirming its ultra-highly chemical stability (Figure 4b and Figure S27, Supporting Information). Variable temperature PXRD patterns revealed that ZJU-74 shows an excellent thermal stability up to 300 °C without phase changes observed

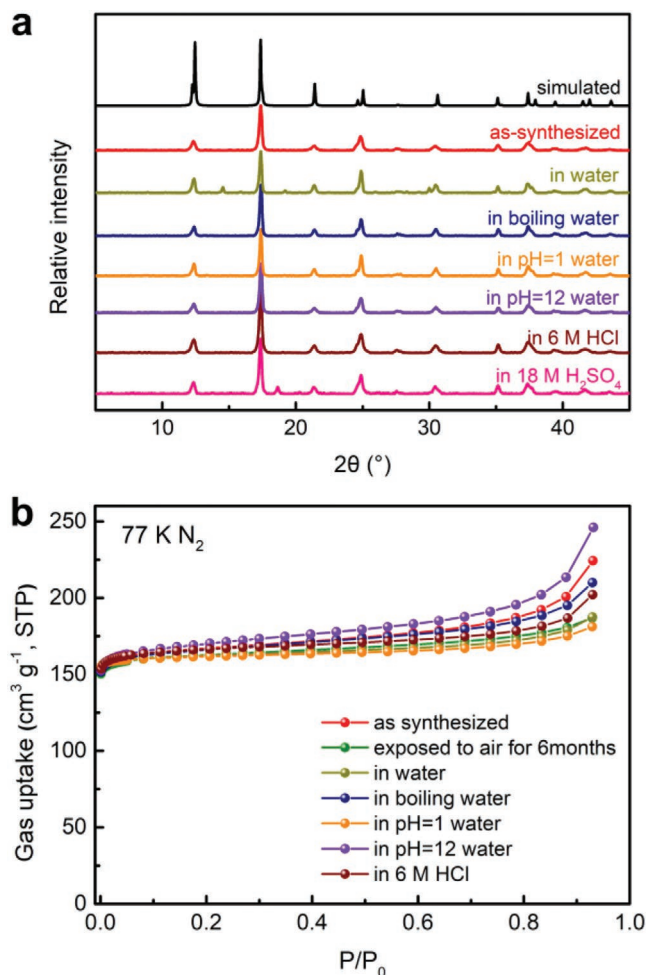


Figure 4. a) PXRD patterns of ZJU-74 samples after treatment with different conditions. b) N_2 adsorption isotherms at 77 K of ZJU-74a after treatment under different conditions, indicating its highly chemical stability.

(Figure S28, Supporting Information). To be able to compare the materials, we also tested the chemical stability of some top-performing C_2H_2 -selective MOFs and stable MOFs reported, including UTSA-74, Zn-MOF-74, TIFSIX-2-Cu-i, UiO-66, ZIF-8, and so on (Table S2, Supporting Information). On the basis of the PXRD analysis and literature report (Figures S29–S35, Supporting Information), ZJU-74a shows the best chemical stability among the indicated MOFs, even comparable to some of the state-of-the-art MOFs and COFs.^[25] Furthermore, bulk samples of ZJU-74 are easily synthesized and scaled up from commercially available and inexpensive reagents by using a fast and direct mixing method at room temperature, as inferred from the PXRD (Figures S36 and S37, Supporting Information). Overall, by virtue of the specifically designed sandwich-like binding sites of a known, chemically-stable, ultramicroporous MOF made by common and inexpensive reagents, highly efficient capture of C_2H_2 from various other gases has been realized for promising energy-efficient separation technologies.

In summary, we reported that a chemically stable Hofmann-type MOF (ZJU-74a), featuring record-high density of OMSs and unique sandwich-like binding sites, exhibits a new benchmark for C_2H_2 capture at low pressure. This maximizes the C_2H_2 -related separation performance, affording the highest C_2H_2/CO_2 selectivity for robust MOFs reported so far and very high C_2H_2/C_2H_4 and C_2H_2/CH_4 selectivities. We attribute this ultrastrong C_2H_2 capture capacity to the unique sandwich-like binding environments, in which the oppositely adjacent open metal centers and cyanide groups from adjacent $[Ni(CN)_4]^{2-}$ units can dually and synergistically interact with C_2H_2 molecule and thus provide the very strong binding affinity for C_2H_2 , as indicated by theoretical calculations. Simulated and breakthrough experiments demonstrated that ZJU-74a can efficiently capture and separate C_2H_2 from C_2H_2/CO_2 (dry and wet), C_2H_2/C_2H_4 and C_2H_2/CH_4 mixtures, respectively. Combined with its extraordinary water/pH stability and easy synthesis from common and inexpensive reagents, ZJU-74 represents a new benchmark material that has the potential to be applied for industrial challenges related to C_2H_2 separation. Our work not only reports the benchmark porous material for C_2H_2 capture and separation, but also provides a new approach to the development of porous materials with strong C_2H_2 binding affinity to address some relevant and challenging gas separations.

Experimental Section

Synthesis of $Co(pyrazine)[Ni(CN)_4]$ (ZJU-74): An aqueous solution of $K_2[Ni(CN)_4] \cdot nH_2O$ (3 mL, 0.125 mmol) was slowly and carefully layered with a methanol/aqueous solution (1/1, 5 mL) of $Co(NO_3)_2 \cdot 6H_2O$ (0.125 mmol) and pyrazine (pyz, 0.125 mmol) using a methanol/water buffer solution (2/3, 4 mL). Orange square-block-shaped single crystals of ZJU-74 were synthesized at room temperature after two weeks. An alternative fast and direct mixing method was used to produce large amount of powder samples of ZJU-74. An aqueous solution (2 mL) of $K_2[Ni(CN)_4] \cdot nH_2O$ (0.5 mmol) was added to a methanol/water solution (1/1, 10 mL) of $Co(NO_3)_2 \cdot 6H_2O$ (0.5 mmol) and pyz (0.5 mmol) at 30 °C, and the resulted light pink precipitate was obtained under constant stirring for 3 h (78% yield based on pyz).

A micromeritics ASAP 2020 surface area analyzer was used to measure gas adsorption isotherms. Kinetic and equilibrium adsorption and desorption were measured by the Intelligent Gravimetric Analyzer

(IGA001, Hiden, UK) under diverse operating conditions. To remove all the guest solvents in the framework, the fresh powder samples were first solvent-exchanged with dry acetone at least 10 times within two days, and evacuated at room temperature (296 K) for 24 h and further at 363 K for 12 h until the outgas rate was 5 mmHg min⁻¹ prior to measurements. The sorption measurement was maintained at 77 K under liquid nitrogen bath. Julabo water bath was used to keep the adsorption tube at a constant temperature of 273, 288, 296, 313, and 333 K, respectively.

Single-crystal X-ray diffraction data of ZJU-74 were collected on an Agilent Supernova CCD diffractometer equipped with graphite-monochromatic enhanced Mo-K α radiation ($\lambda = 0.71073 \text{ \AA}$) at 100 K. The datasets were corrected by empirical absorption correction using spherical harmonics, implemented in the SCALE3 ABSPACK scaling algorithm. The structure was solved by direct methods and refined by full matrix least-squares methods with the SHELX-97 program package.^[26] The pyridine ligand is disordered. The crystal data are summarized in Table S3, Supporting Information.

The breakthrough experiments were performed in dynamic gas breakthrough equipment using a stainless steel column (4.0 mm inner diameter \times 120 mm). The weight of sample packed in the column was: 0.8329 g. The mixed gas flows of (1) dry and wet $C_2H_2/CO_2 = 50/50$ (v/v), (2) $C_2H_2/C_2H_4 = 1/99$ (v/v), (3) $C_2H_2/CH_4 = 50/50$ (v/v), and (4) $C_2H_2/C_2H_6 = 50/50$ (v/v) were then introduced at 2 mL min⁻¹. The desorption test of ZJU-74a was conducted under a sweeping He gas with a flow of 10 mL min⁻¹ at 373 K. Outlet gas from the column was monitored using gas chromatography (GC-2014C, SHIMADZU) with a thermal conductivity detector (TCD, detection limit 0.1 ppm). The standard gases were used to calibrate the concentration of the outlet gas. After the breakthrough tests, ZJU-74a can be readily regenerated by sweeping He gas (10 mL min⁻¹) at 373 K for 30 min.

Supporting Information

Supporting Information is available from the Wiley Online Library or from the author.

Acknowledgements

B.L. acknowledges the support of the National Science Foundation of China (51803179), the “National 1000 Young Talent Program”, and the “Zhejiang University 100 Talent Program”

Conflict of Interest

The authors declare no conflict of interest.

Keywords

acetylene capture, gas separation, Hofmann-type, porous materials, sandwich-like binding

Received: December 17, 2019

Revised: April 8, 2020

Published online: May 11, 2020

[1] P. J. Stang, F. Diederich, *Modern Acetylene Chemistry*, Wiley-VCH, Weinheim, Germany **1995**.

[2] J. C. W. Chien, *Polyacetylene Chemistry, Physics, and Material Science*, Academic Press, London, UK **1984**.

[3] A. Granada, S. B. Karra, S. M. Senkan, *Ind. Eng. Chem. Res.* **1987**, 26, 1901.

- [4] a) H. Molero, B. F. Bartlett, W. T. Tysoe, *J. Catal.* **1999**, *181*, 49; b) H. Molero, D. Stacchiola, W. T. Tysoe, *Catal. Lett.* **2005**, *101*, 145.
- [5] N. S. Schbib, M. A. García, C. E. Gígola, A. F. Errazu, *Ind. Eng. Chem. Res.* **1996**, *35*, 1496.
- [6] J. D. Lewis, *US patent 3837144*, **1974**.
- [7] a) H. Furukawa, K. E. Cordova, M. O'Keeffe, O. M. Yaghi, *Science* **2013**, *341*, 974; b) K. Adil, Y. Belmabkhout, R. S. Pillai, A. Cadiau, P. M. Bhatt, A. H. Assen, G. Maurin, M. Eddaoudi, *Chem. Soc. Rev.* **2017**, *46*, 3402; c) X. Zhao, Y. Wang, D. S. Li, X. Bu, P. Feng, *Adv. Mater.* **2018**, *30*, 1705189; d) M. I. Gonzalez, A. B. Turkiewicz, L. E. Darago, J. Oktawiec, K. Bustillo, F. Grandjean, G. J. Long, J. R. Long, *Nature* **2020**, *577*, 64; e) P. Li, N. A. Vermeulen, C. D. Malliakas, D. A. Gómez-Gualdrón, A. J. Howarth, B. L. Mehdi, A. Dohnalkova, N. D. Browning, M. O'Keeffe, O. K. Farha, *Science* **2017**, *356*, 624; f) T. Kundu, M. Wahiduzzaman, B. B. Shah, G. Maurin, D. Zhao, *Angew. Chem., Int. Ed.* **2019**, *58*, 8073.
- [8] a) D.-D. Zhou, P. Chen, C. Wang, S.-S. Wang, Y. Du, H. Yan, Z.-M. Ye, C.-T. He, R.-K. Huang, Z.-W. Mo, N.-Y. Huang, J.-P. Zhang, *Nat. Mater.* **2019**, *18*, 994; b) H.-G. Hao, Y.-F. Zhao, D.-M. Chen, J.-M. Yu, K. Tan, S. Ma, Y. Chabal, Z.-M. Zhang, J.-M. Dou, Z.-H. Xiao, G. Day, H.-C. Zhou, T.-B. Lu, *Angew. Chem., Int. Ed.* **2018**, *57*, 16067; c) A. Cadiau, K. Adil, P. M. Bhatt, Y. Belmabkhout, M. Eddaoudi, *Science* **2016**, *353*, 137; d) H. Wang, X. Dong, V. Colombo, Q. Wang, Y. Liu, W. Liu, X.-L. Wang, X.-Y. Huang, D. M. Proserpio, A. Sironi, Y. Han, J. Li, *Adv. Mater.* **2018**, *30*, 1805088; e) Z. Niu, X. Cui, T. Pham, P. C. Lan, H. Xing, K. A. Forrest, L. Wojtas, B. Space, S. Ma, *Angew. Chem., Int. Ed.* **2019**, *58*, 10138; f) Z. Y. Dong, Y. Z. S. Sun, J. Chu, X. Z. Zhang, H. X. Deng, *J. Am. Chem. Soc.* **2017**, *139*, 14209.
- [9] a) H. Wang, X. Dong, J. Lin, S. J. Teat, S. Jensen, J. Cure, E. V. Alexandrov, Q. Xia, K. Tan, Q. Wang, D. H. Olson, D. M. Proserpio, Y. J. Chabal, T. Thonhauser, J. Sun, Y. Han, J. Li, *Nat. Commun.* **2018**, *9*, 1745; b) W.-G. Cui, T.-L. Hu, X.-H. Bu, *Adv. Mater.* **2019**, *31*, 1806445; c) S. Yang, A. J. Ramirez-Cuesta, R. Newby, V. Garcia-Sakai, P. Manuel, S. K. Callear, S. I. Campbell, C. C. Tang, M. Schröder, *Nat. Chem.* **2015**, *7*, 121; d) I. M. Hçnricke, I. Senkovska, V. Bon, I. A. Baburin, N. Bçnisch, S. Raschke, J. D. Evans, S. Kaskel, *Angew. Chem., Int. Ed.* **2018**, *57*, 13780; e) S. Dang, Q.-L. Zhu, Q. Xu, *Nat. Rev. Mater.* **2017**, *3*, 17075; f) Y. X. Wang, S. B. Peh, D. Zhao, *Small* **2019**, *15*, 1900058.
- [10] a) X. Cui, K. Chen, H. Xing, Q. Yang, R. Krishna, Z. Bao, H. Wu, W. Zhou, X. Dong, Y. Han, B. Li, Q. Ren, M. J. Zaworotko, B. Chen, *Science* **2016**, *353*, 141; b) K.-J. Chen, D. G. Madden, S. Mukherjee, T. Pham, K. A. Forrest, A. Kumar, B. Space, J. Kong, Q.-Y. Zhang, M. J. Zaworotko, *Science* **2019**, *366*, 241; c) B. Li, X. Cui, D. O'Nolan, H.-M. Wen, M. Jiang, R. Krishna, H. Wu, R.-B. Lin, Y.-S. Chen, D. Yuan, H. Xing, W. Zhou, Q. Ren, G. Qian, M. J. Zaworotko, B. Chen, *Adv. Mater.* **2017**, *29*, 1704210.
- [11] Z. Bao, G. Chang, H. Xing, R. Krishna, Q. Ren, B. Chen, *Energy Environ. Sci.* **2016**, *9*, 3612.
- [12] J.-R. Li, R. J. Kuppler, H.-C. Zhou, *Chem. Soc. Rev.* **2009**, *38*, 1477.
- [13] a) O. T. Qazvini, R. Babarao, S. G. Telfer, *Chem. Mater.* **2019**, *31*, 4919; b) Y.-P. Li, Y. Wang, Y.-Y. Xue, H.-P. Li, Q.-G. Zhai, S.-N. Li, Y.-C. Jiang, M.-C. Hu, X. Bu, *Angew. Chem., Int. Ed.* **2019**, *58*, 13590; c) M. L. Foo, R. Matsuda, Y. Hijikata, R. Krishna, H. Sato, S. Horike, A. Hori, J. Duan, Y. Sato, Y. Kubota, M. Takata, S. Kitagawa, *J. Am. Chem. Soc.* **2016**, *138*, 3022; d) R.-B. Lin, L. Li, H. Wu, H. Arman, B. Li, R.-G. Lin, W. Zhou, B. Chen, *J. Am. Chem. Soc.* **2017**, *139*, 8022; e) H. Zeng, M. Xie, Y.-L. Huang, Y. Zhao, X.-J. Xie, J.-P. Bai, M.-Y. Wan, R. Krishna, W. Lu, D. Li, *Angew. Chem., Int. Ed.* **2019**, *58*, 8515.
- [14] a) Y. Ye, Z. Ma, R.-B. Lin, R. Krishna, W. Zhou, Q. Lin, Z. Zhang, S. Xiang, B. Chen, *J. Am. Chem. Soc.* **2019**, *141*, 4130; b) F. Moreau, I. da Silva, N. H. Al Smail, T. L. Easun, M. Savage, H. G. W. Godfrey, S. F. Parker, P. Manuel, S. Yang, M. Schröder, *Nat. Commun.* **2017**, *8*, 14085; c) H. S. Scott, M. Shivanna, A. Bajpai, D. G. Madden, K.-J. Chen, T. Pham, K. A. Forrest, A. Hogan, B. Space, J. J. Perry, M. J. Zaworotko, *ACS Appl. Mater. Interfaces* **2017**, *9*, 33395.
- [15] a) J. Lee, C. Y. Chuah, J. Kim, Y. Kim, N. Ko, Y. Seo, K. Kim, T. H. Bae, E. Lee, *Angew. Chem., Int. Ed.* **2018**, *57*, 7869; b) K.-J. Chen, H. S. Scott, D. G. Madden, T. Pham, A. Kumar, A. Bajpai, M. Lusi, K. A. Forrest, B. Space, J. J. Perry, M. J. Zaworotko, *Chem* **2016**, *1*, 753; c) Z. Yao, Z. Zhang, L. Liu, Z. Li, W. Zhou, Y. Han, B. Chen, R. Krishna, S. Xiang, *Chem. - Eur. J.* **2016**, *22*, 5676.
- [16] a) J.-P. Zhang, A.-X. Zhu, R.-B. Lin, X.-L. Qi, X.-M. Chen, *Adv. Mater.* **2011**, *23*, 1268; b) H.-M. Wen, H. Wang, B. Li, Y. Cui, H. Wang, G. Qian, B. Chen, *Inorg. Chem.* **2016**, *55*, 7214; c) J. Pang, F. Jiang, M. Wu, C. Liu, K. Su, W. Lu, D. Yuan, M. Hong, *Nat. Commun.* **2015**, *6*, 7575.
- [17] a) S. Xiang, W. Zhou, Z. Zhang, M. A. Green, Y. Liu, B. Chen, *Angew. Chem., Int. Ed.* **2010**, *49*, 4615; b) S. Xiang, W. Zhou, J. M. Gallegos, Y. Liu, B. Chen, *J. Am. Chem. Soc.* **2009**, *131*, 12415.
- [18] a) E. D. Bloch, W. L. Queen, R. Krishna, J. M. Zadrozny, C. M. Brown, J. R. Long, *Science* **2012**, *335*, 1606; b) Y.-S. Bae, C. Y. Lee, K. C. Kim, O. K. Farha, P. Nickias, J. T. Hupp, S. T. Nguyen, R. Q. Snurr, *Angew. Chem., Int. Ed.* **2012**, *51*, 1857.
- [19] F. Luo, C. S. Yan, L. L. Dang, R. Krishna, W. Zhou, H. Wu, X. L. Dong, Y. Han, T.-L. Hu, M. O'Keeffe, L. L. Wang, M. B. Luo, R.-B. Lin, B. Chen, *J. Am. Chem. Soc.* **2016**, *138*, 5678.
- [20] Y.-L. Peng, T. Pham, P. Li, T. Wang, Y. Chen, K.-J. Chen, K. A. Forrest, B. Space, P. Cheng, M. J. Zaworotko, Z. Zhang, *Angew. Chem., Int. Ed.* **2018**, *57*, 10971.
- [21] a) Y. Niel, J. M. Martinez-Agudo, M. C. Munoz, A. B. Gaspar, J. A. Real, *Inorg. Chem.* **2001**, *40*, 3838; b) Y. Li, Y. Liu, Y. Wang, Y. Leng, L. Xie, X. Li, *Int. J. Hydrogen Energy* **2007**, *32*, 3411; c) J. T. Culp, M. R. Smith, E. Bittner, B. Bockrath, *J. Am. Chem. Soc.* **2008**, *130*, 12427; d) M. M. Deshmukh, M. Ohba, S. Kitagawa, S. Sakaki, *J. Am. Chem. Soc.* **2013**, *135*, 4840.
- [22] P. Li, Y. He, Y. Zhao, L. Weng, H. Wang, R. Krishna, H. Wu, W. Zhou, M. O'Keeffe, Y. Han, B. Chen, *Angew. Chem., Int. Ed.* **2015**, *54*, 574.
- [23] a) K. Weissermel, H.-J. Arpe, *Industrial Organic Chemistry*, 4th ed., Wiley-VCH, Weinheim, Germany **2003**; b) N. P. Revsbech, J. Sørensen, *Denitrification in Soil and Sediment*, Plenum Press, New York **1990**.
- [24] K. M. Sundaram, M. M. Shreehan, E. F. Olszewski, "Ethylene," in *Firk-Othmer Encyclopedia of Chemical Technology*, Wiley, New York **2001**.
- [25] a) S. Yuan, L. Feng, K. Wang, J. Pang, M. Bosch, C. Lollar, Y. Sun, J. Qin, X. Yang, P. Zhang, Q. Wang, L. Zou, Y. Zhang, L. Zhang, Y. Fang, J. Li, H.-C. Zhou, *Adv. Mater.* **2018**, *30*, 1704303; b) B. Wang, X.-L. Lv, D. Feng, L.-H. Xie, J. Zhang, M. Li, Y. Xie, J.-R. Li, H.-C. Zhou, *J. Am. Chem. Soc.* **2016**, *138*, 6204; c) X. Guan, H. Li, Y. Ma, M. Xue, Q. Fang, Y. Yan, V. Valtchev, S. Qiu, *Nat. Chem.* **2019**, *11*, 587.
- [26] G. M. Sheldrick, *SHELXL-97, Program for the Refinement of Crystal Structures*, University of Göttingen, Göttingen, Germany **1997**.

ADVANCED MATERIALS

Supporting Information

for *Adv. Mater.*, DOI: 10.1002/adma.201908275

A Chemically Stable Hofmann-Type Metal#Organic Framework with Sandwich-Like Binding Sites for Benchmark Acetylene Capture

Jiyan Pei, Kai Shao, Jia-Xin Wang, Hui-Min Wen, Yu Yang, Yuanjing Cui, Rajamani Krishna, Bin Li, and Guodong Qian**

Supplementary Information

A Chemically Stable Hofmann-Type Metal–Organic Framework with Sandwich-Like Binding Sites for Benchmark Acetylene Capture

Jiyan Pei, Kai Shao, Jia-Xin Wang, Hui-Min Wen, Yu Yang, Yuanjing Cui, Rajamani Krishna, Bin Li, and Guodong Qian**

J. Pei, K. Shao, J.-X. Wang, Dr. Y. Yang, Prof. Y. Cui, Prof. B. Li, Prof. G. Qian

State Key Laboratory of Silicon Materials, Cyrus Tang Center for Sensor Materials and Applications, Department of Materials Science & Engineering, Zhejiang University, Hangzhou 310027, China

E-mail: bin.li@zju.edu.cn; gdqian@zju.edu.cn

Dr. H.-M. Wen

College of Chemical Engineering, Zhejiang University of Technology, Zhejiang, 310014, China

Prof. R. Krishna

Van't Hoff Institute for Molecular Sciences, University of Amsterdam, Science Park 904, 1098 XH Amsterdam, Netherlands

1. General Materials and MOF Synthesis

All starting chemicals and solvents were purchased from commercial companies cheaply and could be directly used without further purification. Among them, cobalt(II) nitrate hexahydrate ($\text{Co}(\text{NO}_3)_2 \cdot 6\text{H}_2\text{O}$, CAS: 10026-22-9) was purchased from Sinopharm with the price of USD 9.8 per 100 g, pyrazine (pyz, CAS: 290-37-9) was purchased from Energy Chemical with the price of USD 22.9 per 100 g, and potassium tetracyanonickelate(II) hydrate ($\text{K}_2[\text{Ni}(\text{CN})_4] \cdot n\text{H}_2\text{O}$, CAS: 339527-86-5) was purchased from Heowns with the price of USD 45 per 10 g. Thermogravimetric analyses (TGA) were examined by using a Netzsch TG209F3 under N_2 atmosphere with a heating rate of 5 K min^{-1} . Powder X-ray diffraction (PXRD) patterns were collected in the $2\theta = 2\text{-}45^\circ$ range on an X'Pert PRO diffractometer with $\text{Cu K}\alpha$ ($\lambda = 1.542 \text{ \AA}$) radiation at room temperature.

N_2 (99.999%), C_2H_2 (99.6%), CO_2 (99.999%), C_2H_4 (99.9%), CH_4 (99.995%), C_2H_6 (99.99%), He (99.999%) and mixed gases of (1) $\text{C}_2\text{H}_2/\text{CO}_2 = 50/50$ (v/v), (2) $\text{C}_2\text{H}_2/\text{C}_2\text{H}_4 = 1/99$ (v/v), (3) $\text{C}_2\text{H}_2/\text{CH}_4 = 50/50$ (v/v), $\text{C}_2\text{H}_2/\text{C}_2\text{H}_6 = 50/50$ (v/v) were purchased from JinGong Company (China).

2. Fitting of pure component isotherms

The pure component isotherm data for C_2H_2 , CO_2 , C_2H_4 , CH_4 and C_2H_6 in ZJU-74a were fitted with the dual-site Langmuir-Freundlich isotherm model

$$q = q_{A,\text{sat}} \frac{b_A p^{\nu_A}}{1 + b_A p^{\nu_A}} + q_{B,\text{sat}} \frac{b_B p^{\nu_B}}{1 + b_B p^{\nu_B}} \quad (1)$$

with T-dependent parameters b_A , and b_B

$$b_A = b_{A0} \exp\left(\frac{E_A}{RT}\right); \quad b_B = b_{B0} \exp\left(\frac{E_B}{RT}\right) \quad (2)$$

The fitted parameter values are presented in Table S4.

3. Isotheric heat of adsorption

A virial-type expression of comprising the temperature-independent parameters a_i and b_j was employed to calculate the enthalpies of adsorption for C_2H_2 (at 296, 313 and 333 K), CO_2 , C_2H_4 , CH_4 and C_2H_6 (at 273, 296 and 313 K) on ZJU-74a. In each case, the data were fitted use equation:

$$\ln P = \ln N + 1/T \sum_{i=0}^m a_i N_i + \sum_{j=0}^n b_j N_j$$

(3)

Here, P is the pressure expressed in mmHg, N is the amount absorbed in mmol g^{-1} , T is the temperature in K, a_i and b_j are virial coefficients, and m , n represent the number of coefficients required to adequately describe the isotherms (m and n were gradually increased till the contribution of extra added a and b coefficients was deemed to be statistically insignificant towards the overall fit. And the average value of the squared deviations from the experimental values was minimized). The values of the virial coefficients a_0 through a_m were then used to calculate the isosteric heat of absorption using the following expression:

$$Q_{st} = -R \sum_{i=0}^m a_i N_i$$

(4)

Q_{st} is the coverage-dependent isosteric heat of adsorption and R is the universal gas constant. The heat enthalpy of C_2H_2 , CO_2 , C_2H_4 and CH_4 sorption for complex ZJU-74a in this manuscript are determined by using the sorption data measured in the pressure range from 0-1 bar (at 296, 313 and 333 K for C_2H_2 , at 273, 296 and 313 K for CO_2 , C_2H_4 , CH_4 and C_2H_6 , respectively).

4. IAST calculations of adsorption selectivities

We consider the separation of binary C_2H_2/CO_2 , C_2H_2/C_2H_4 , C_2H_2/CH_4 and C_2H_2/C_2H_6 mixtures. The adsorption selectivity for C_2H_2/CO_2 , C_2H_2/C_2H_4 , C_2H_2/CH_4 and C_2H_2/C_2H_6 separation is defined by

$$S_{ads} = \frac{q_1/q_2}{p_1/p_2}$$

(5)

In equation (5), q_1 and q_2 are the molar loadings in the adsorbed phase in equilibrium with the bulk gas phase with partial pressures p_1 , and p_2 . IAST calculations of the adsorption selectivity of 50/50 (v/v) C_2H_2/CO_2 , 1/99 (v/v) C_2H_2/C_2H_4 , 50/50 (v/v) C_2H_2/CH_4 , and 50/50 and 1/99 (v/v) C_2H_2/C_2H_6 mixtures are shown in Figure 2e and S38e, respectively.

5. Computational results and details

In order to obtain a reasonable binding site of gas molecules in ZJU-74a for subsequent modeling, the Grand Canonical Monte Carlo (GCMC) simulations were performed in the MS modeling. The crystal structures of ZJU-74a were chosen for related simulations without further geometry optimization. The framework and the individual C_2H_2 , CO_2 and C_2H_4 molecules were considered to be rigid during the simulation. Partial charges for atoms of guest-free ZJU-74a were derived from QEq method and QEq_neutral1.0 parameter. The simulations were carried out at 298 K, adopting the locate task, Metropolis method in Sorption module and the universal force field (UFF). The partial charges on the atoms of C_2H_2 (C: $-0.129e$; H1: $0.129e$, where $e = 1.6022 \times 10^{-19}$ C is the elementary charge), CO_2 (C: $0.894e$; O: $-0.447e$) and C_2H_4 (C: $-0.301e$; H: $0.151e$) were also derived from QEq method. The interaction energy between hydrocarbon molecules and framework were computed through the Coulomb and Lennard-Jones 6-12 (LJ) potentials. The cutoff radius was chosen as 12.5 \AA for the LJ potential and the long-range electrostatic interactions were handled using the Ewald & Group summation method. The loading steps and the equilibration steps were 1×10^5 , the production steps were 1×10^6 . The binding energy between the framework and gas molecule was calculated using: $\Delta E = E_{(MOF)} + E_{(gas)} - E_{(MOF+gas)}$. Note that the pyz ligand rotational flexibility/dynamics, which could not be accounted for in our ordered structural models, may also play some role on gas adsorption. Despite of this limitation, our calculations still provide helpful qualitative insights on the gas binding mechanisms.

6. Transient breakthrough simulations

The performance of industrial fixed bed adsorbers is dictated by a combination of adsorption selectivity and uptake capacity. Transient breakthrough simulations were carried out for

C₂H₂/CO₂ (50/50, v/v), C₂H₂/C₂H₄ (1/99, v/v) and C₂H₂/CH₄ (50/50, v/v) separations operating at a total pressure of 100 kPa and 296 K, using the methodology described in earlier publications.¹⁻⁴ For the breakthrough simulations, the following parameter values were used: length of packed bed, $L = 0.3$ m; voidage of packed bed, $\varepsilon = 0.4$; superficial gas velocity at inlet, $u = 0.04$ m/s.

The transient breakthrough simulation results are presented in terms of a *dimensionless* time, $\tau = \frac{tu}{L\varepsilon}$, defined by dividing the actual time, t , by the characteristic time, $\frac{L\varepsilon}{u}$. The y -axis is the dimensionless concentration of each species at the exit of the adsorber, c_A divided by the inlet concentrations of that species, c_{A0} .

7. Kinetic and equilibrium adsorption measurement

Kinetic and equilibrium adsorption were measured with the Intelligent Gravimetric Analyzer (IGA001, Hiden, UK), which uses a gravimetric technique to accurately measure the gas sorption on materials under diverse operating conditions. About 50 mg of ZJU-74a sample was loaded into the sample cell, then the system was outgassed at 393 K for 2 h prior to the gas sorption measurements. All the gases used (C₂H₂, CO₂, and He) were of 99.99% purity.

8. Gas equilibrium adsorption capacity and separation factor

The complete breakthrough of C₂H₂ was indicated by the downstream gas composition reaching that of the feed gas. On the basis of the mass balance, the gas adsorption capacities can be determined as follows:

$$q_i = \frac{c_i V}{22.4 \times m} \times \int_0^t \left(1 - \frac{F}{F_0}\right) dt \quad (6)$$

Where q_i is the equilibrium adsorption capacity of gas i (mmol g⁻¹), C_i is the feed gas concentration, V is the volumetric feed flow rate (cm³ min⁻¹), t is the adsorption time (min), F_0 and F are the inlet and outlet gas molar flow rates, respectively, and m is the mass of the adsorbent (g). The separation factor (α) of the breakthrough experiment is determined as:

$$\alpha = \frac{q_A y_B}{q_B y_A} \quad (7)$$

in which y_i is the molar fraction of gas i ($i = A, B$) in the gas mixture.

Notation

| | |
|------------------|---|
| b | Langmuir-Freundlich constant, $\text{kPa}^{-\nu}$ |
| q | component molar loading of species i , mol kg^{-1} |
| q_{sat} | saturation loading, mol kg^{-1} |
| L | length of packed bed adsorber, m |
| t | time, s |
| T | absolute temperature, K |
| u | superficial gas velocity in packed bed, m s^{-1} |

Greek letters

| | |
|---------------|--------------------------------------|
| ε | voidage of packed bed, dimensionless |
| ν | Freundlich exponent, dimensionless |
| τ | time, dimensionless |

Table S1. Comparison of the C₂H₂ adsorption uptake, C₂H₂/CO₂ selectivity, and heat of adsorption data in ZJU-74a with some top-performing C₂H₂-selective materials reported.

| Porous materials | C ₂ H ₂ uptake (cm ³ g ⁻¹) | | C ₂ H ₂ /CO ₂ selectivity ^a | C ₂ H ₂ Q_{st} (kJ mol ⁻¹) ^b | Refs |
|------------------|---|-------------|---|---|------------------|
| | 0.01 bar | 0.5 bar | | | |
| ZJU-74a | 49 | 76.7 | 36.5 | 45-65^c | This work |
| NKMOF-1-Ni | 39 | 55.5 | 22 | 60.3 | 5 |
| HOF-3a | 4.6 | 42.5 | 21.5 | 39.3 | 6 |
| DICRO-4-Ni-i | 9.7 | 36.3 | 13.9 | 37.7 | 7 |
| JCM-1 | 10.1 | 63.5 | 13.7 | 36.9 | 8 |
| UTSA-74a | 19.2 | 88.9 | 9 | 33 | 9 |
| SNNU-45 | 19.7 | 114.1 | 8.5 | 39.9 | 10 |
| SIFSIX-3-Ni | 4.5 | 65.7 | 7.7 | 36.7 | 11 |
| TIFSIX-2-Cu-i | 39.9 | 83 | 6.5 | 46.3 | 11 |
| FJU-90 | 7.7 | 154.53 | 4.3 | 25.2 | 12 |
| JNU-1 | 5.5 | 53 | 3.6 | 13 | 13 |
| Zn-MOF-74a | 14.7 | 102 | 2.8 | 31.7 | 14 |
| UTSA-200a | 41 | 76.4 | - | 40 | 15 |

^a IAST selectivity for 50/50 (v/v) C₂H₂/CO₂ mixture at 1 bar.

^b Q_{st} values at low surface coverage.

^c The highest Q_{st} values at various surface coverage.

Table S2. Comparison of the chemical stability of ZJU-74 with some stable MOFs and C₂H₂-selective MOFs after treatment under various chemical environments.

| | MOFs | Water | Boiling water | pH=1 | pH=12 | 6M HCl | 18M H ₂ SO ₄ | Refs |
|--|---------------|----------------|----------------|----------------|----------------|----------------|------------------------------------|------------------|
| Stable MOFs | UiO-66 | √ | √ | √ | √ | × | × | 16 |
| | ZIF-8 | √ | √ | × | √ | × | × | 17 |
| | bio-MOF-1 | √ | √ | × | √ | × | × | 18 |
| C ₂ H ₂ /CO ₂ separation MOFs | ZJU-74 | √ | √ | √ | √ | √ | √ | This work |
| | UTSA-74 | × | × | × | × | × | × | 9 |
| | Zn-MOF-74 | √ | × | × | √ | × | × | 14 |
| | TIFSIX-2-Cu-i | × | × | × | × | × | × | 11 |
| | SIFSIX-3-Ni | × | × | × | × | × | × | 11 |
| | UTSA-300 | × | × | × | × | × | × | 19 |
| | HOF-3 | × | × | × | × | × | × | 6 |
| | NKMOF-1-Ni | √ | - ^a | √ | √ | - ^a | - ^a | 5 |
| | JCM-1 | √ | - ^a | - ^a | - ^a | - ^a | - ^a | 8 |
| | FJU-90 | √ | - ^a | - ^a | - ^a | - ^a | - ^a | 12 |
| JNU-1 | √ | - ^a | × | √ | - ^a | - ^a | 13 | |

^a The stability in the corresponding conditions was not reported in the literatures.

Table S3. Crystallographic data and structure refinement results of ZJU-74.

| Unit cell parameters | ZJU-74 |
|--|---|
| Formula | C ₈ H ₄ CoN ₆ Ni |
| Formula weight | 301.81 |
| Temperature (K) | 100(2) |
| Crystal system | Tetragonal |
| Space group | <i>P</i> 4/ <i>mmm</i> |
| <i>a</i> , <i>b</i> (Å) | 7.2201(5) |
| <i>c</i> (Å) | 7.1079(6) |
| α (°) | 90.00 |
| β (°) | 90.00 |
| γ (°) | 90.00 |
| <i>V</i> (Å ³) | 370.53(6) |
| <i>Z</i> | 1 |
| <i>D</i> _{calcd} (g cm ⁻³) | 1.353 |
| μ (mm ⁻¹) | 2.373 |
| <i>F</i> (000) | 149 |
| Crystal size (mm ³) | 0.36 × 0.32 × 0.18 |
| GOF | 1.148 |
| <i>R</i> _{int} | 0.0216 |
| <i>R</i> ₁ , <i>wR</i> ₂ [<i>I</i> ≥ 2σ (<i>I</i>)] | 0.0383, 0.1288 |
| <i>R</i> ₁ , <i>wR</i> ₂ [all data] | 0.0392, 0.1300 |
| Largest diff. peak and hole | 1.478 and -0.289 e/Å ⁻³ |
| CCDC number | 1970545 |

Table S4. Dual-site Langmuir-Freundlich parameter fits for C₂H₂, CO₂, C₂H₄, CH₄ and C₂H₆ in ZJU-74a. The fits are based on experimental isotherm data at 296 K.

| | Site A | | | Site B | | |
|-------------------------------|----------------------|----------------------------------|---------------|----------------------|----------------------------------|---------------|
| | $q_{A,sat}$ | b_{A0} | v_A | $q_{B,sat}$ | b_{B0} | v_B |
| | mol kg ⁻¹ | kPa ^{-v_A} | dimensionless | mol kg ⁻¹ | kPa ^{-v_B} | dimensionless |
| C ₂ H ₂ | 3.49331 | 2.33697 | 0.71987 | 43.27556 | 2.90003×10 ⁻¹¹ | 4.13104 |
| CO ₂ | 5.13027 | 0.00605 | 0.70911 | 3.00942 | 0.02262 | 1.09551 |
| C ₂ H ₄ | 2.03459 | 0.30217 | 1.02859 | 1.21198 | 6.73859×10 ⁻⁴ | 6.54195 |
| CH ₄ | 1.0162 | 0.01091 | 1.02386 | 7.42273 | 5.30806×10 ⁻⁴ | 1.11079 |
| C ₂ H ₆ | 2.71509 | 0.09468 | 1.11565 | 10.26873 | 0.00656 | 0.48961 |

Table S5. The comparison of C₂H₂ and CO₂ uptake capacity of ZJU-74a obtained from single component gas sorption and breakthrough experiments for dry and wet 50/50 C₂H₂/CO₂ mixtures, respectively.

| Sources of data | Gas uptakes (cm ³ g ⁻¹) | | Separation selectivity ^b |
|--|--|-----------------|-------------------------------------|
| | C ₂ H ₂ | CO ₂ | |
| single component gas sorption ^a | 85.7 | 66.3 | - |
| breakthrough experiment under dry gas | 81.5 | 18.8 | 4.3 |
| breakthrough experiment under 60% humidity | 71.4 ^c | 17.6 | 4.1 |

^a Gas uptakes at 296 K and 1.0 bar.

^b The separation selectivity according to breakthrough curve.

^c This value is about 88% of that of breakthrough experiment without humidity.

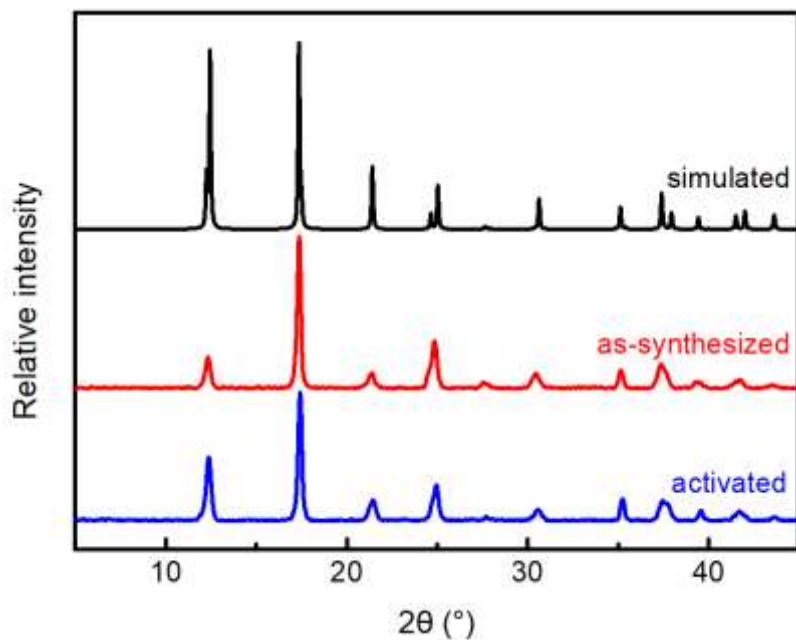


Figure S1. The simulated XRD pattern from the single-crystal X-ray structure of ZJU-74 (black), and the PXRD patterns of as-synthesized powder (red) and activated ZJU-74 (blue) of ZJU-74.

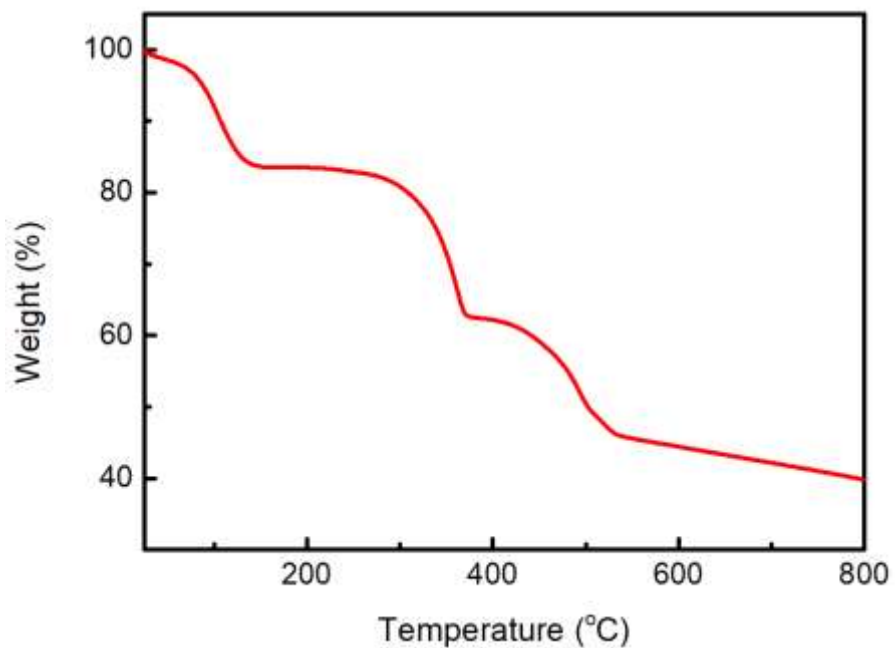


Figure S2. TGA curves of as-synthesized ZJU-74.

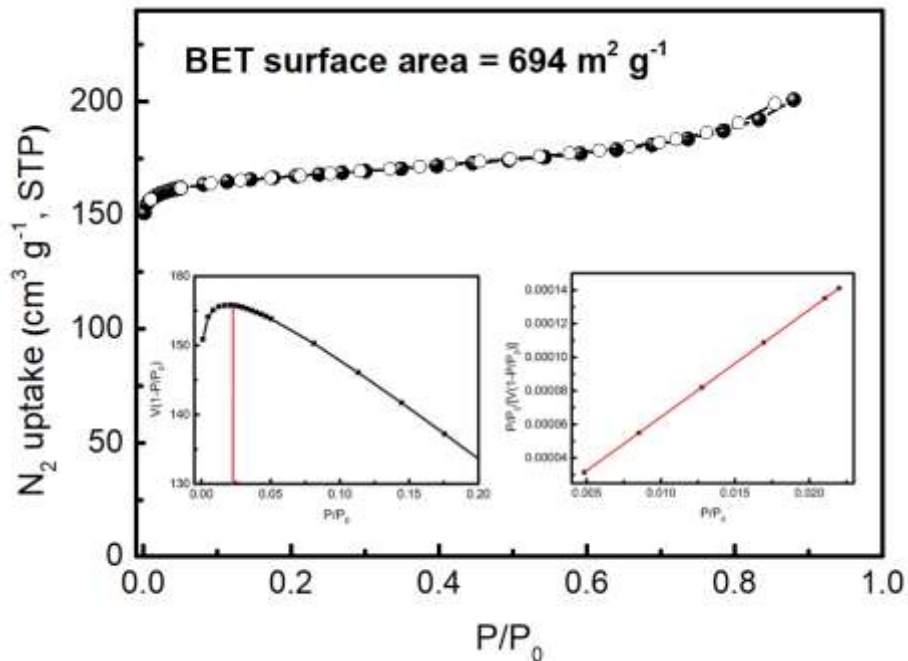


Figure S3. N_2 adsorption isotherms of ZJU-74a at 77 K. Filled/empty symbols represent adsorption/desorption.

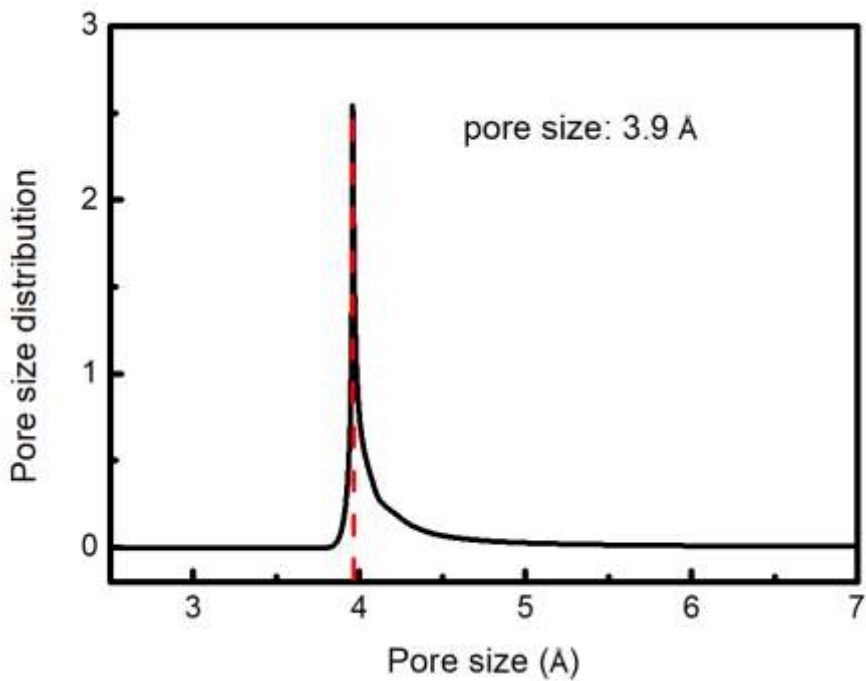


Figure S4. Pore size distribution for ZJU-74a based on Horvath-Kawazoe model.

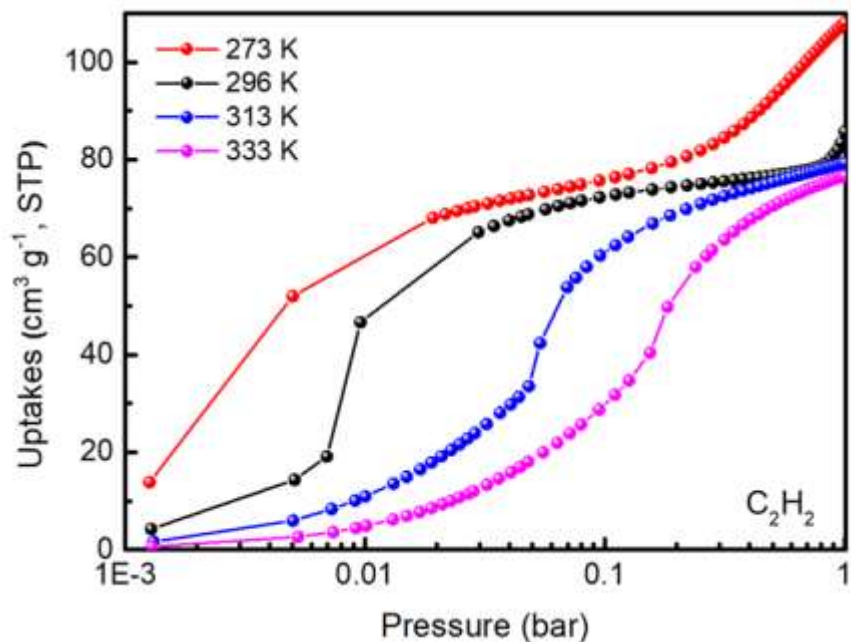


Figure S5. C_2H_2 adsorption isotherms of ZJU-74a at 273 (red), 296 (black), 313 (blue) and 333 K (magenta).

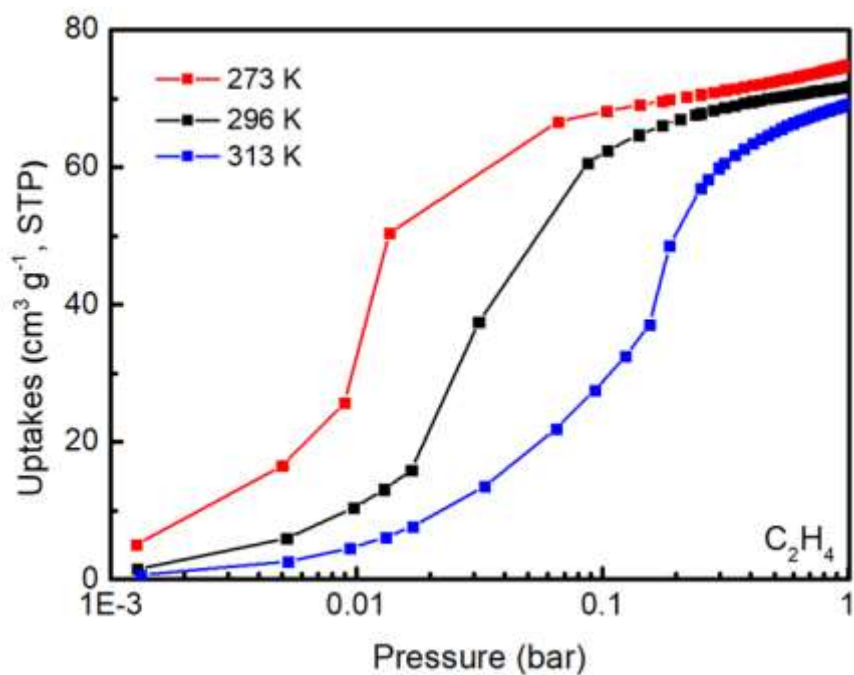


Figure S6. C_2H_4 adsorption isotherms of ZJU-74a at 273 (red), 296 (black) and 313 K (blue).

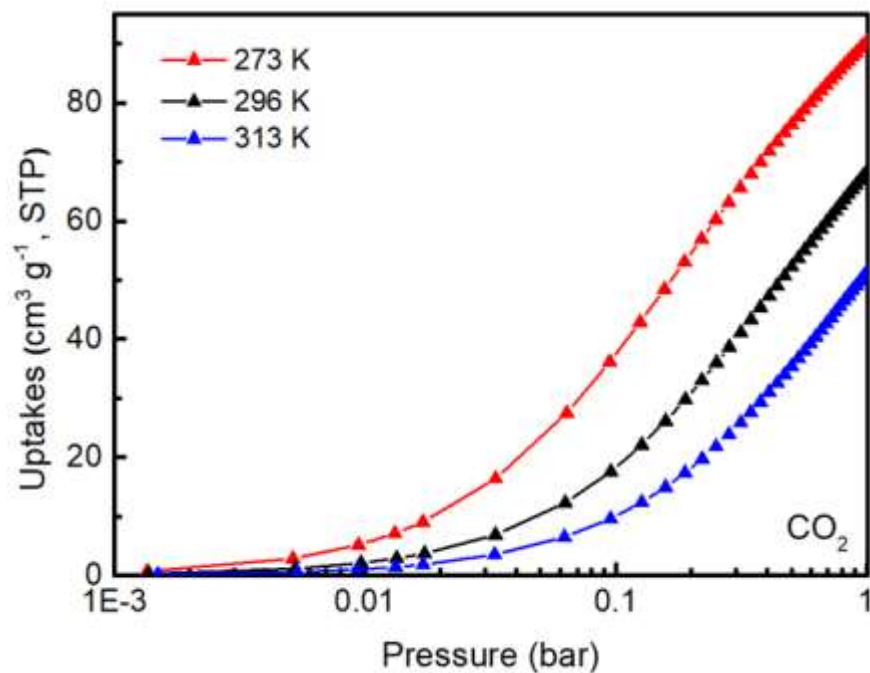


Figure S7. CO₂ adsorption isotherms of ZJU-74a at 273 (red), 296 (black) and 313 K (blue).

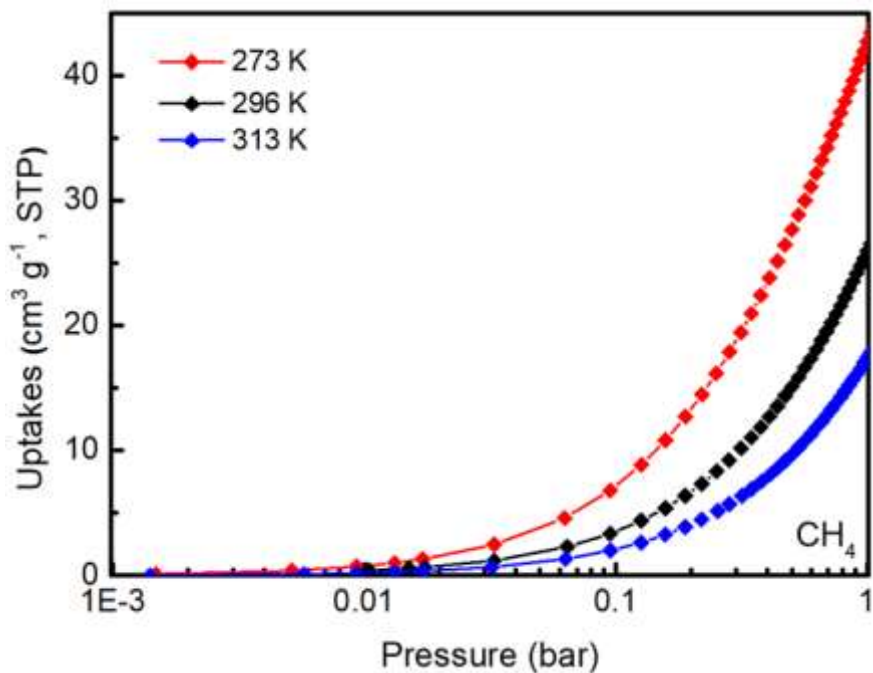


Figure S8. CH₄ adsorption isotherms of ZJU-74a at 273 (red), 296 (black) and 313 K (blue).

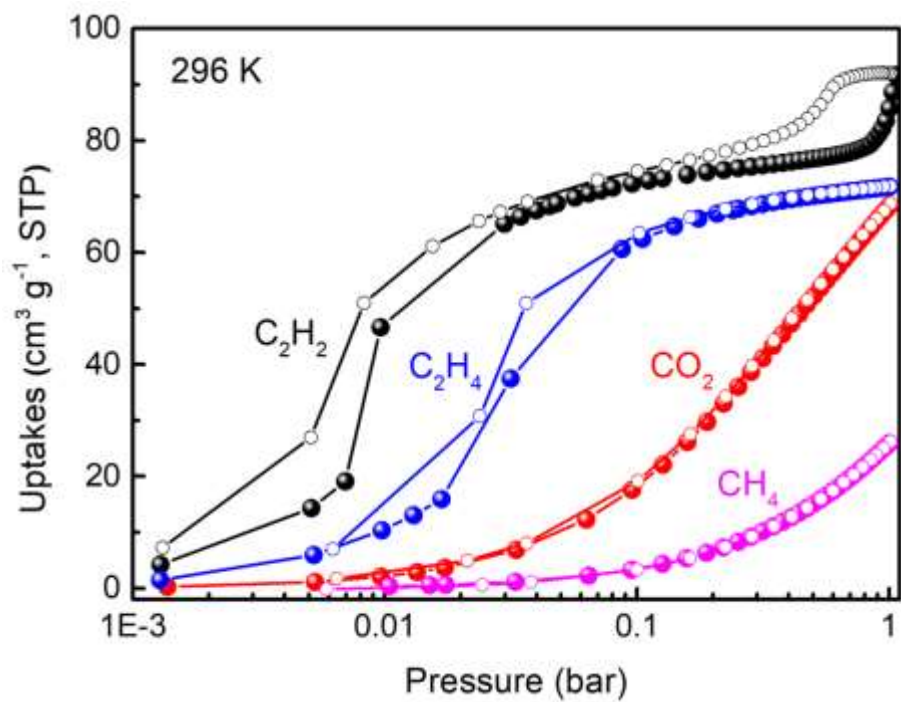


Figure S9. Gas adsorption and desorption isotherms of ZJU-74a for C_2H_2 (black), C_2H_4 (blue), CO_2 (red) and CH_4 (magenta) at 296 K. Filled/empty symbols represent adsorption/desorption.

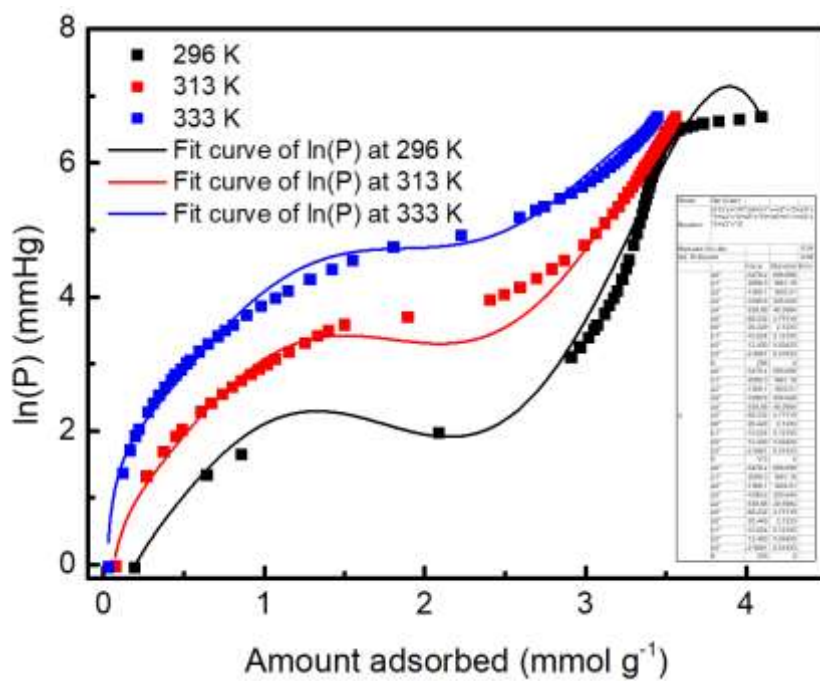


Figure S10. Virial fitting of the C_2H_2 adsorption isotherms for ZJU-74a.

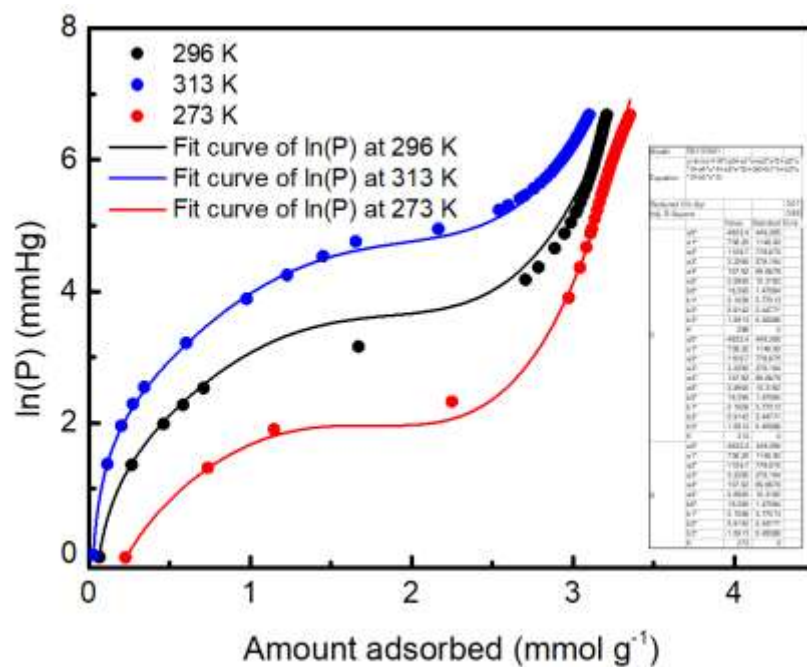


Figure S11. Virial fitting of the C_2H_4 adsorption isotherms for ZJU-74a.

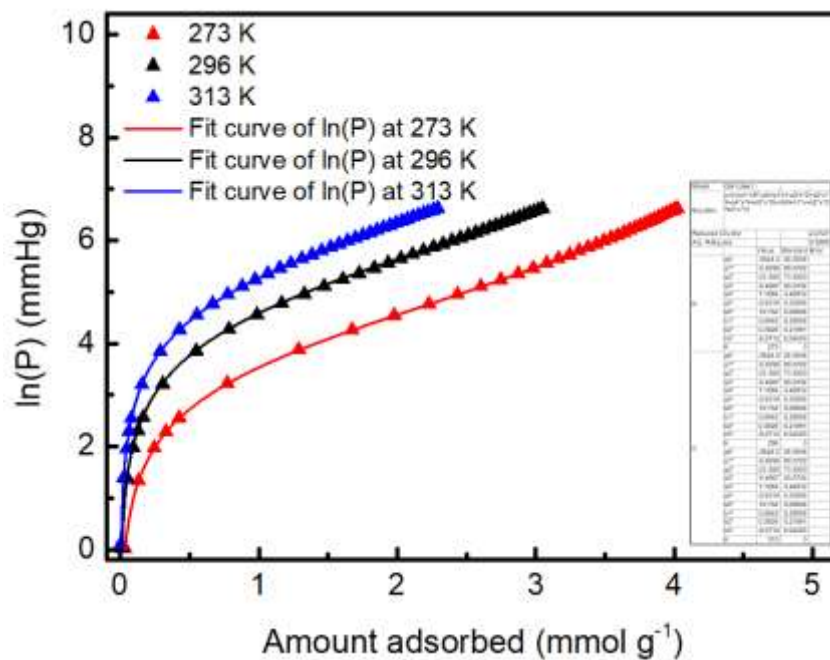


Figure S12. Virial fitting of the CO_2 adsorption isotherms for ZJU-74a.

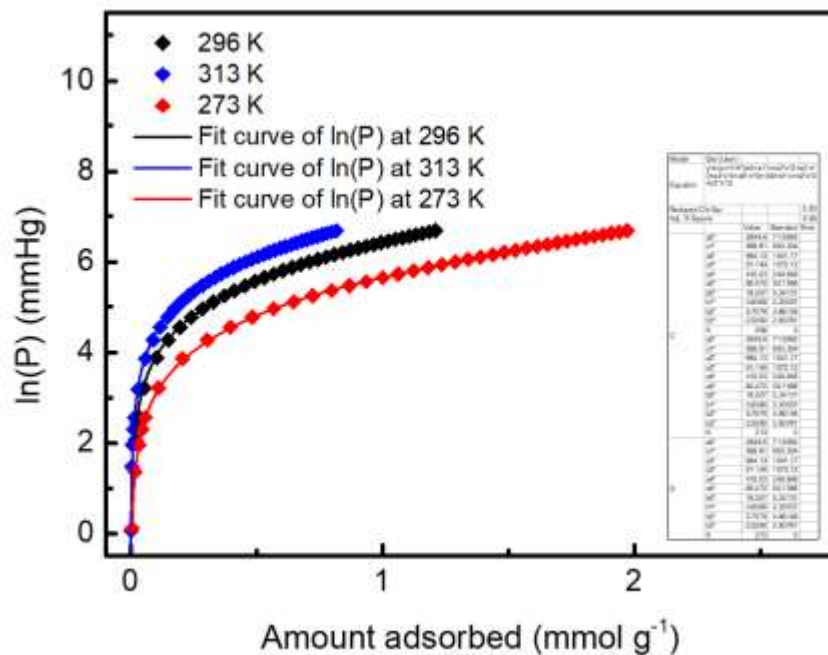


Figure S13. Virial fitting of the CH₄ adsorption isotherms for ZJU-74a.

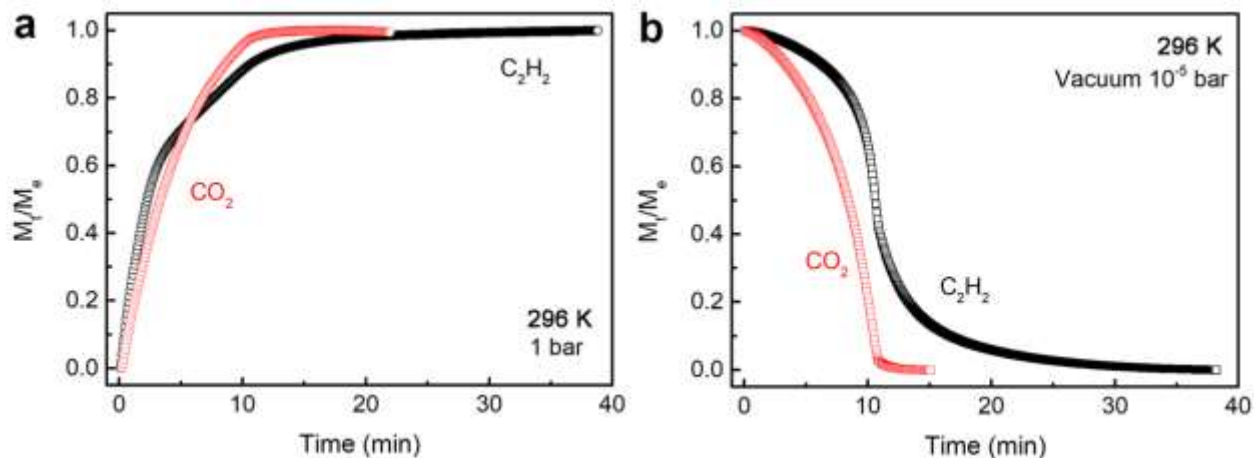


Figure S14. a) Adsorption kinetics profiles of C₂H₂ (black) and CO₂ (red) for ZJU-74a at 296 K. b) Desorption kinetics profiles of C₂H₂ (black) and CO₂ (red) for ZJU-74a at 296 K.

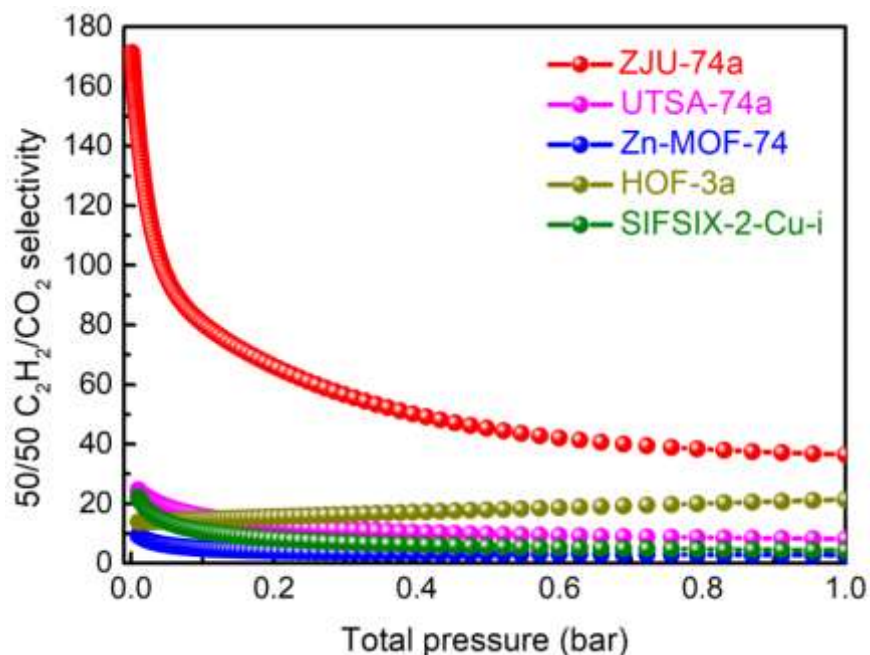


Figure S15. Comparison of the IAST selectivity of ZJU-74a with other top-performing MOF materials for a 50/50 C₂H₂/CO₂ mixture at room temperature.

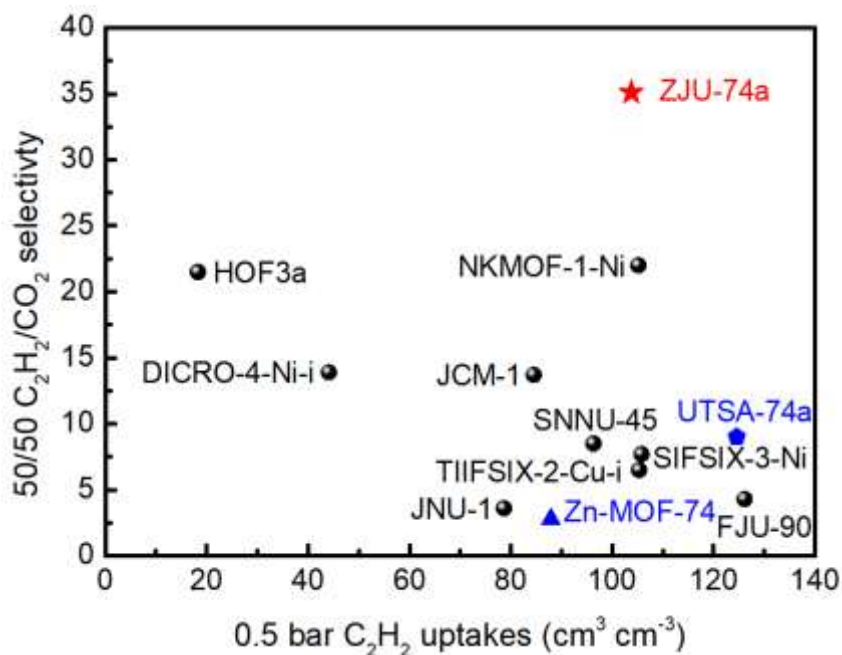


Figure S16. Comparison of the C₂H₂ uptake capacity at 0.5 bar and C₂H₂/CO₂ selectivity for ZJU-74a and other best-performing rigid materials.

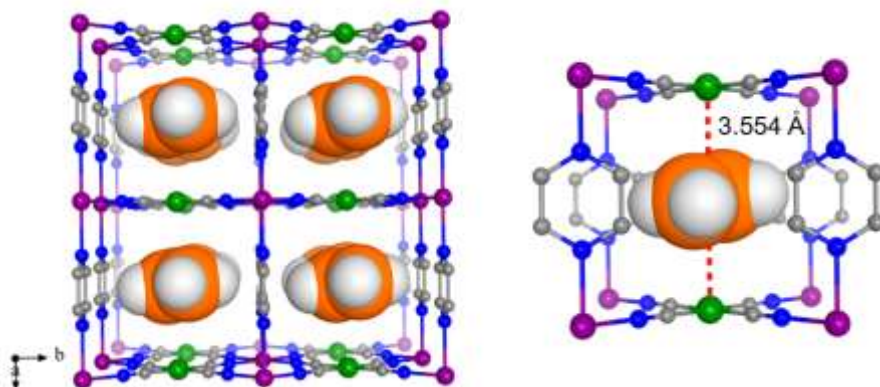


Figure S17. The calculated C_2H_4 molecule binding sites in ZJU-74a. Colour code: Ni (green), Co (purple), N (blue), and C (grey).

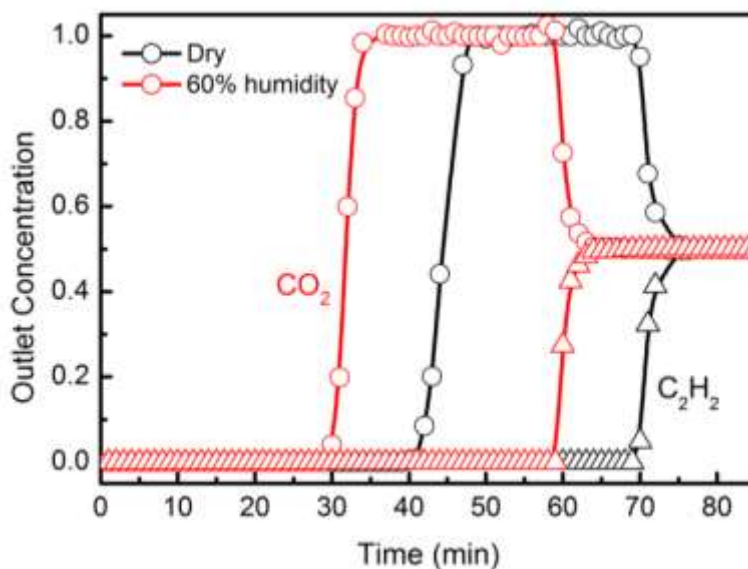


Figure S18. Experimental column breakthrough curves for a wet 50/50 C_2H_2/CO_2 mixture with a total flow of 2 mL min^{-1} in an absorber bed packed with ZJU-74a at 298 K and 1 bar under 60% humidity. Although the τ_{break} of both C_2H_2 and CO_2 move forward due to small amount of OMSs occupied by water molecules, the separation performance of ZJU-74a can be mostly retained with the selectivity of 4.1 and 88% C_2H_2 uptake capacity (dry).

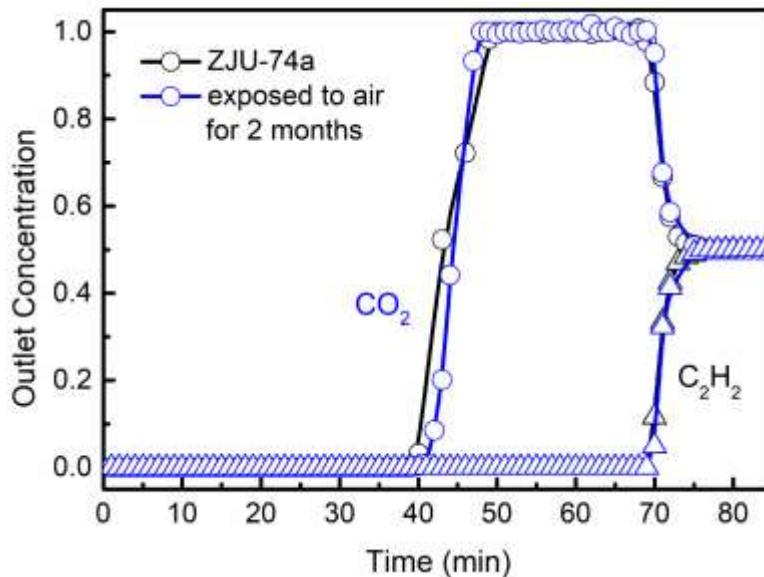


Figure S19. Experimental column breakthrough curves for a 50/50 C_2H_2/CO_2 mixture with a total flow of 2 mL min^{-1} in an absorber bed packed with re-activated ZJU-74a at 298 K and 1 bar, after the sample was exposed to air (50-70% humidity) for 2 months.

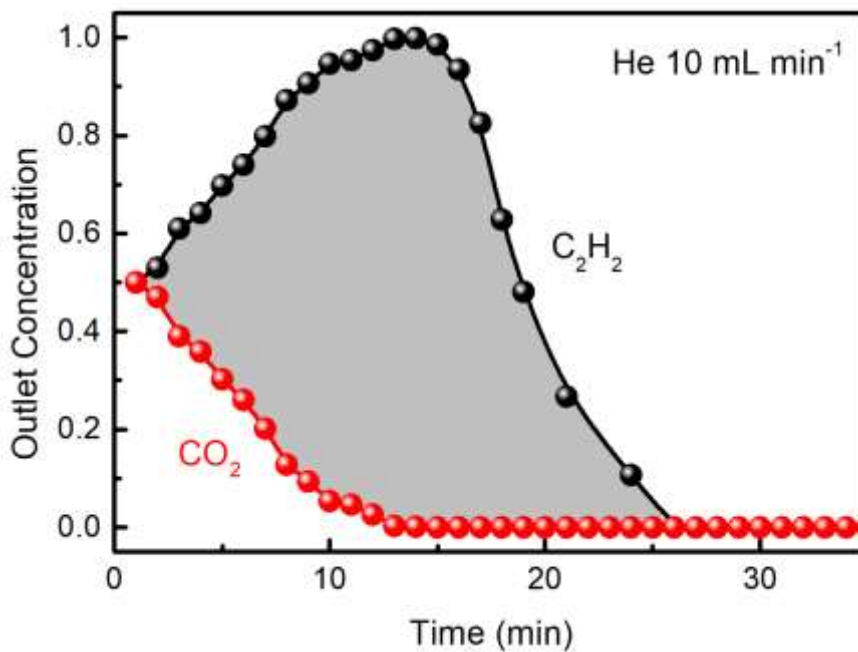


Figure S20. The desorption curves of ZJU-74a under 10 mLmin^{-1} sweeping He gas at 373 K, affording a C_2H_2 recovery of 3.01 mmol g^{-1} with high purity over 91%.

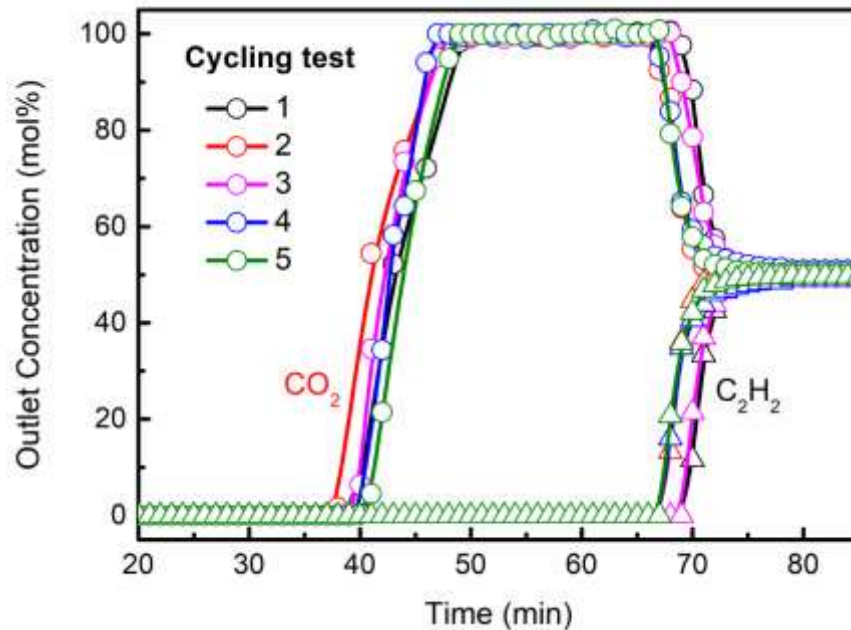


Figure S21. Experimental column breakthrough curves for a cycling test of 50/50 C_2H_2/CO_2 mixture with a total flow of 2 mL min^{-1} in an absorber bed packed with ZJU-74a at 298 K and 1 bar.

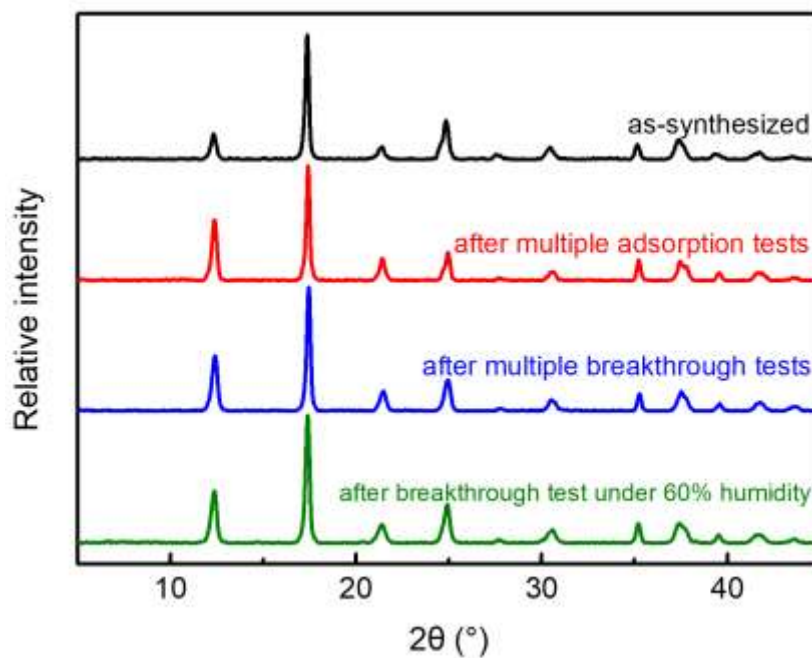


Figure S22. PXRD patterns of as-synthesized samples (black), the samples after the multiple adsorption tests (red), multiple breakthrough tests (blue) and the breakthrough test under 60% humidity (green) of ZJU-74a.

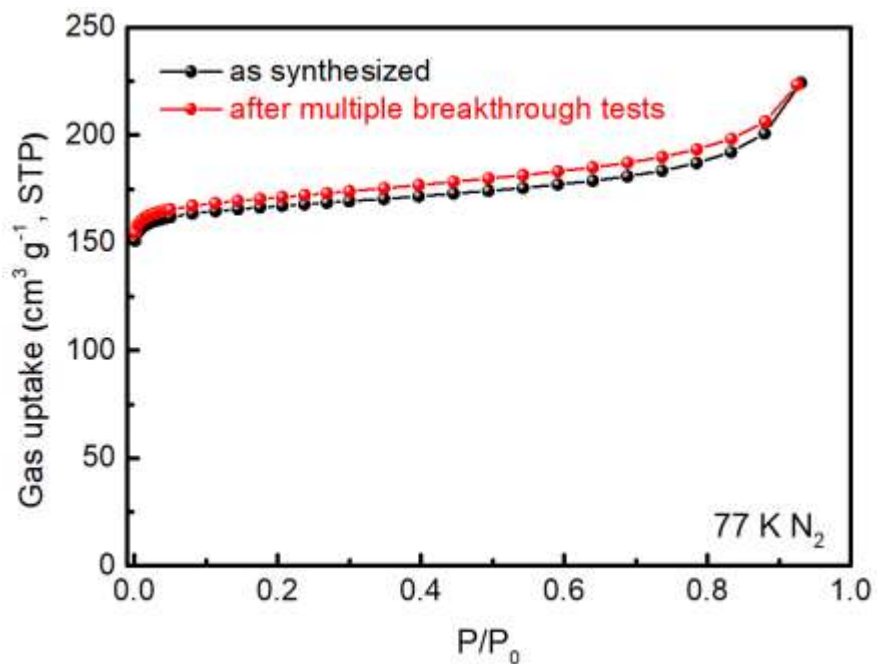


Figure S23. N₂ adsorption isotherms at 77 K of ZJU-74a after multiple breakthrough tests.

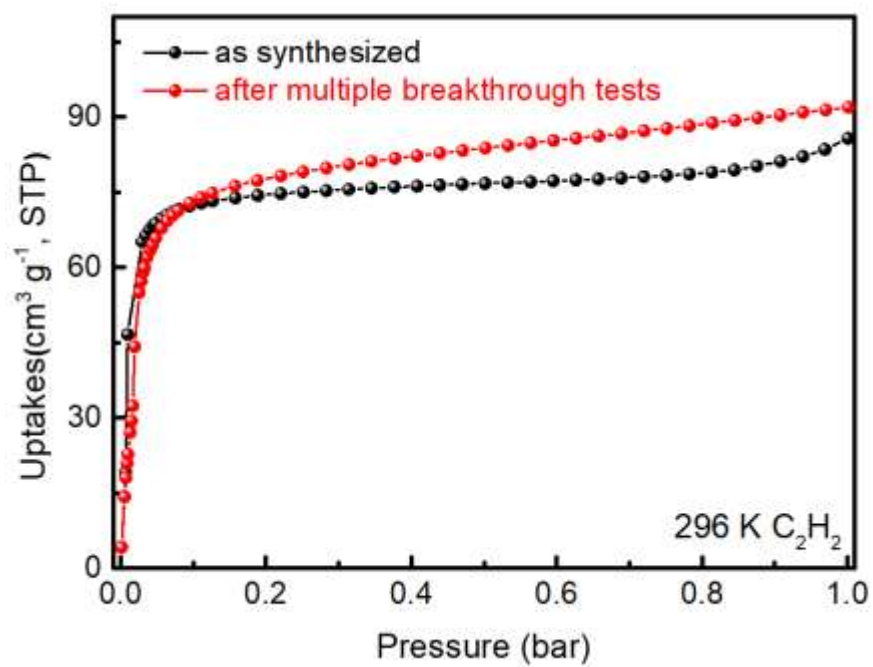


Figure S24. C₂H₂ adsorption isotherms at 296 K of ZJU-74a after multiple breakthrough tests.

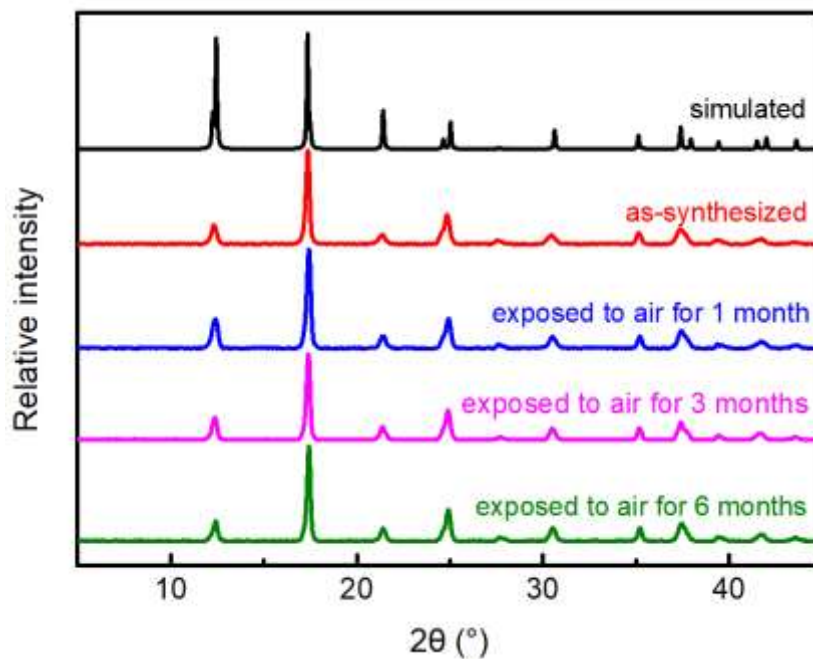


Figure S25. PXRD patterns of simulated, as-synthesized ZJU-74, and ZJU-74 samples exposed to air for 1 month, 3 months and 6 months.

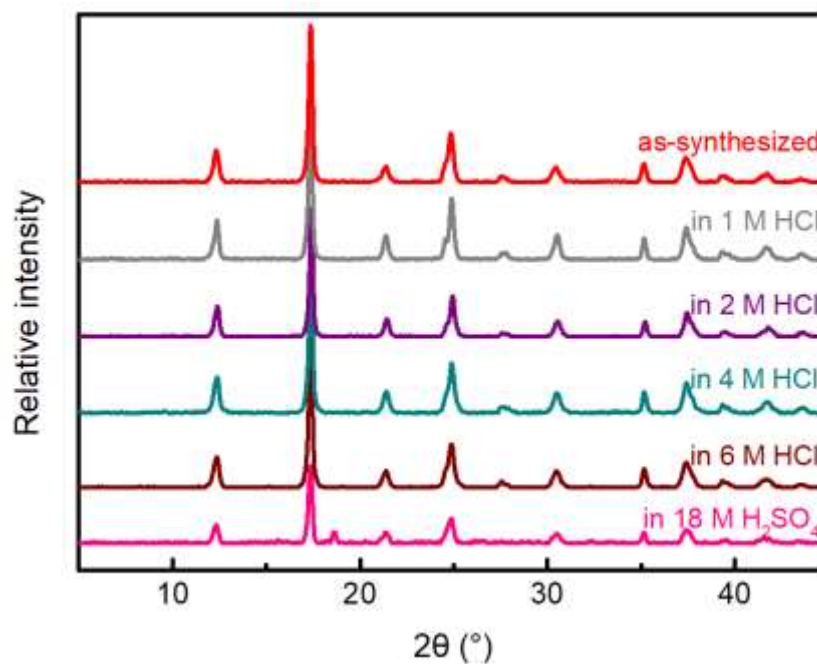


Figure S26. PXRD patterns of ZJU-74 after treatment with 1 M, 2 M, 4 M, 6 M HCl for 3 days and concentrated H₂SO₄ for several hours.

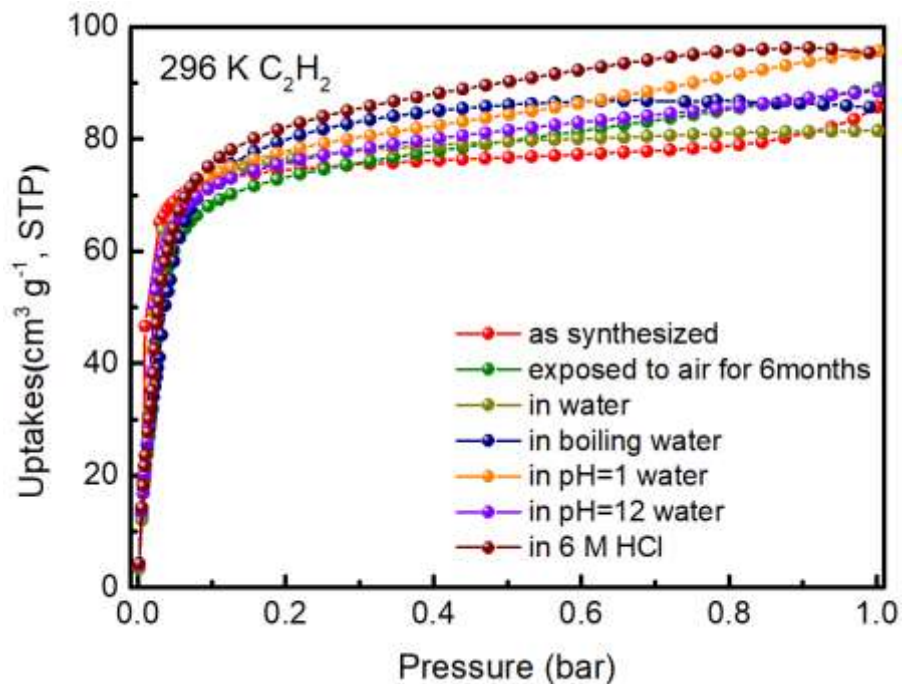


Figure S27. C_2H_2 adsorption isotherms at 296 K of ZJU-74a after treatment under different conditions.

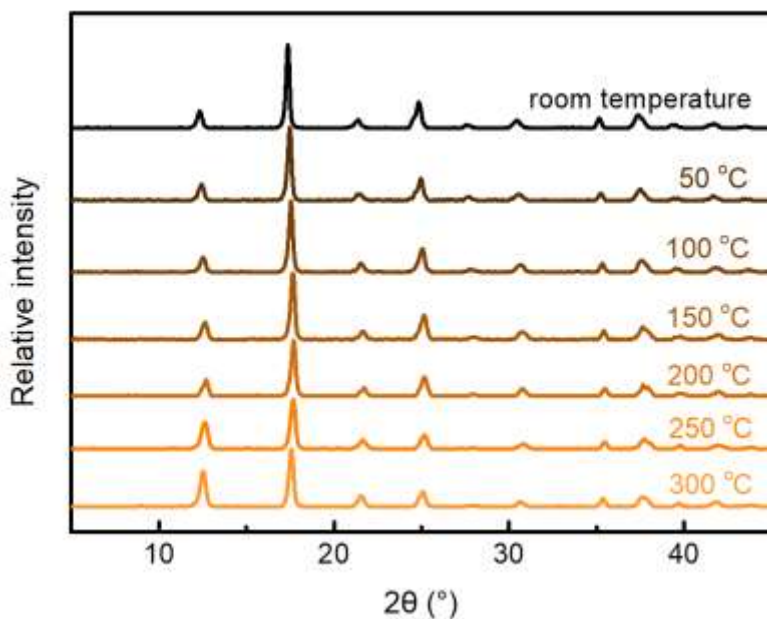


Figure S28. Variable-temperature PXRD patterns for ZJU-74.

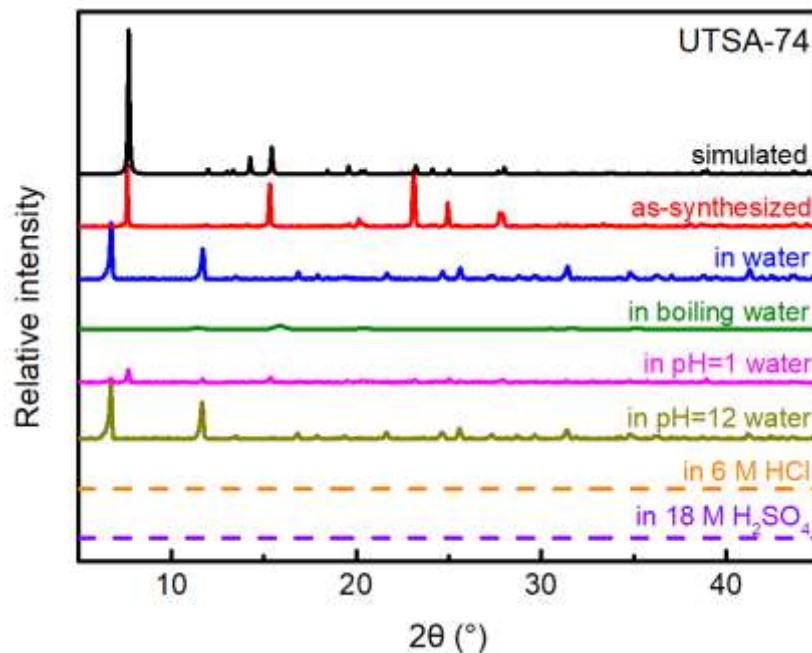


Figure S29. PXRD patterns of UTSA-74 samples after treatment under different conditions, indicating that this framework is not stable under more extreme conditions such as boiling water and pH = 1. Dash lines represent that no solid left after treatment.

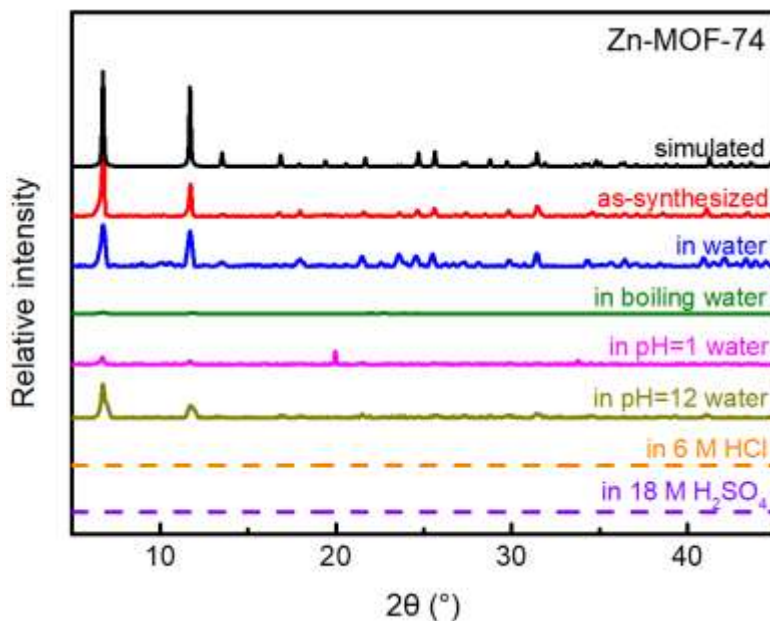


Figure S30. PXRD patterns of Zn-MOF-74 samples after treatment under different conditions, indicating that this framework is not stable under more extreme conditions such as boiling water, pH = 1 and 12. Dash lines represent that no solid left after treatment.

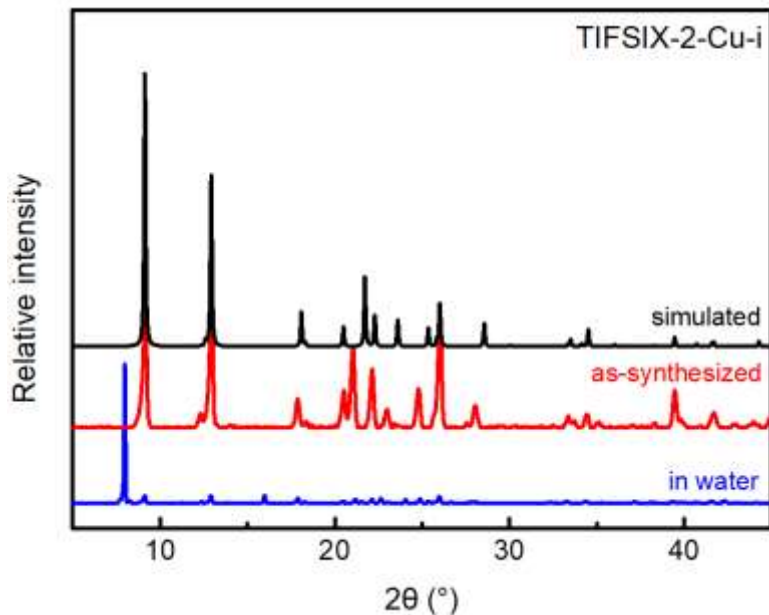


Figure S31. PXRD patterns of TIFSIX-2-Cu-i samples after treatment under different conditions, indicating that this framework is not stable in the water.

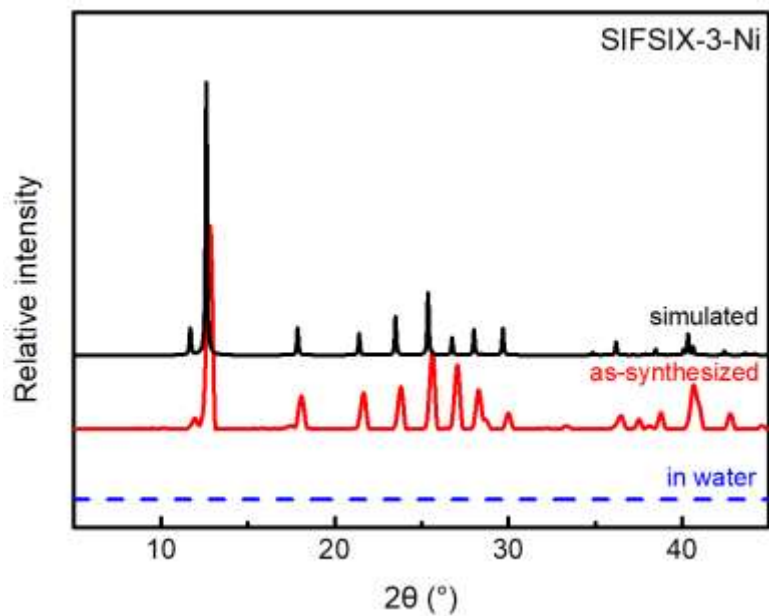


Figure S32. PXRD patterns of SIFSIX-3-Ni samples after treatment under different conditions. Dash line represents that no solid left after treatment and the framework is not stable in the water.

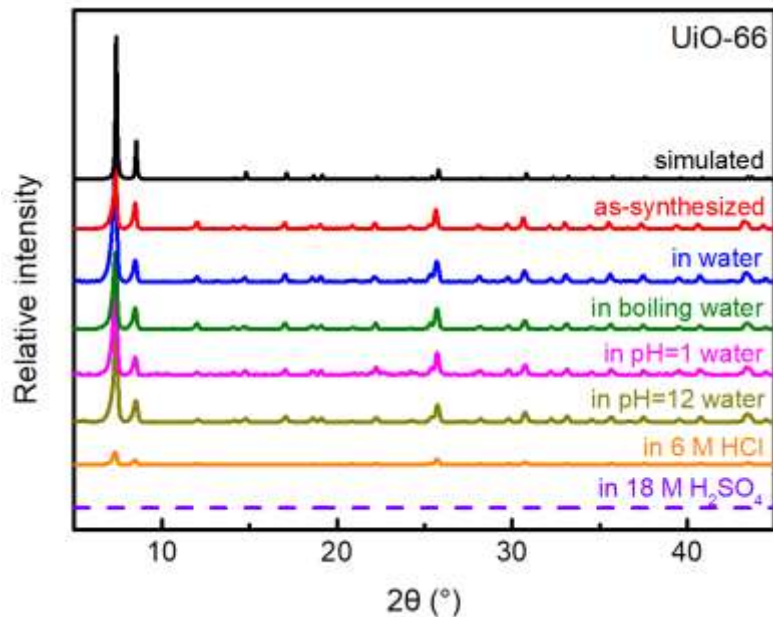


Figure S33. PXRD patterns of UiO-66 samples after treatment under different conditions. Dash line represents that no solid left after treatment and the framework is not stable in 6M HCl and 18 M H₂SO₄.

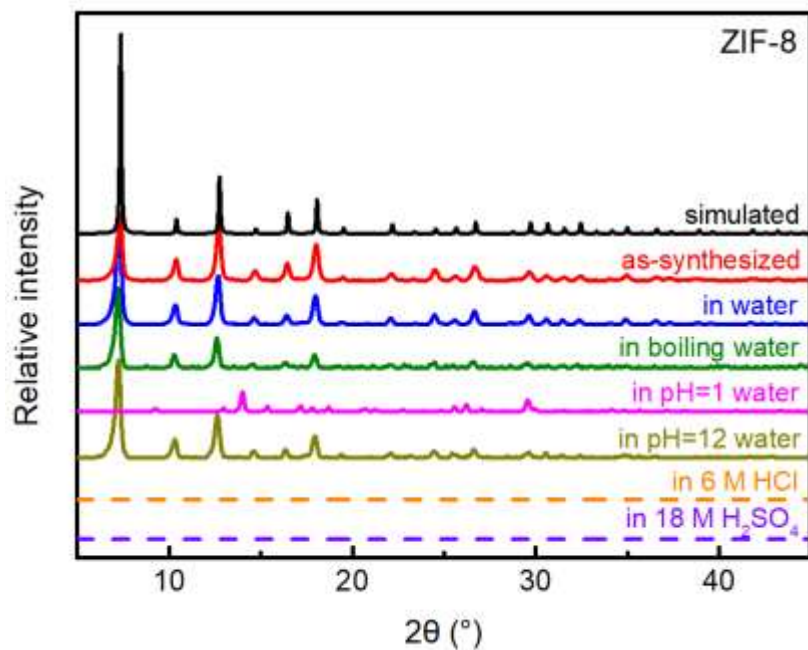


Figure S34. PXRD patterns of ZIF-8 samples after treatment under different conditions, indicating that the framework is not stable under pH = 1 solution. Dash lines represent that no solid left after treatment.

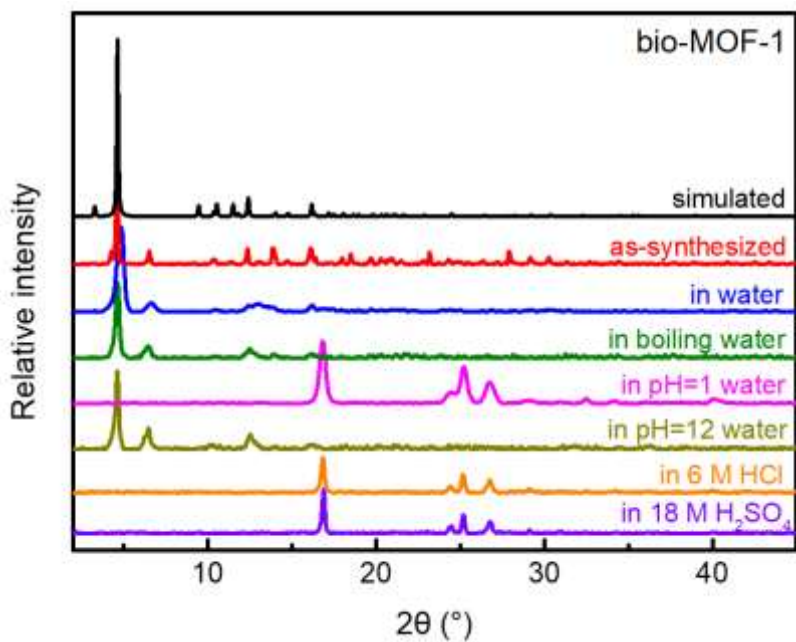


Figure S35. PXRD patterns of bio-MOF-1 samples after treatment under different conditions, indicating that the framework is not stable under pH = 1 solution.

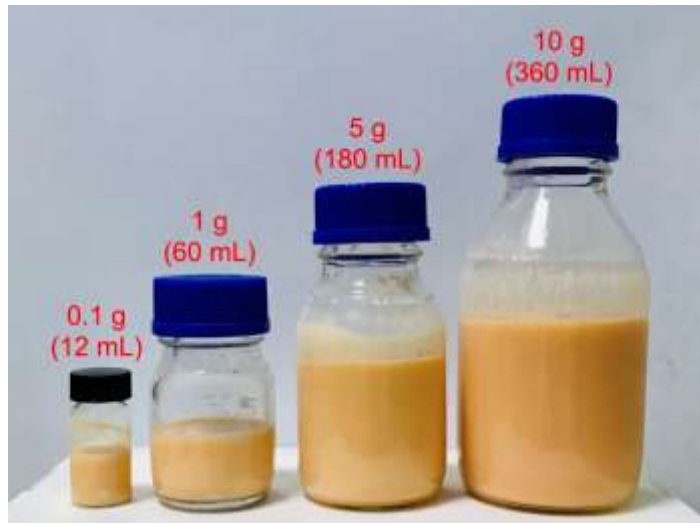


Figure S36. Investigating the scalability of ZJU-74 synthesis by using different content raw materials.

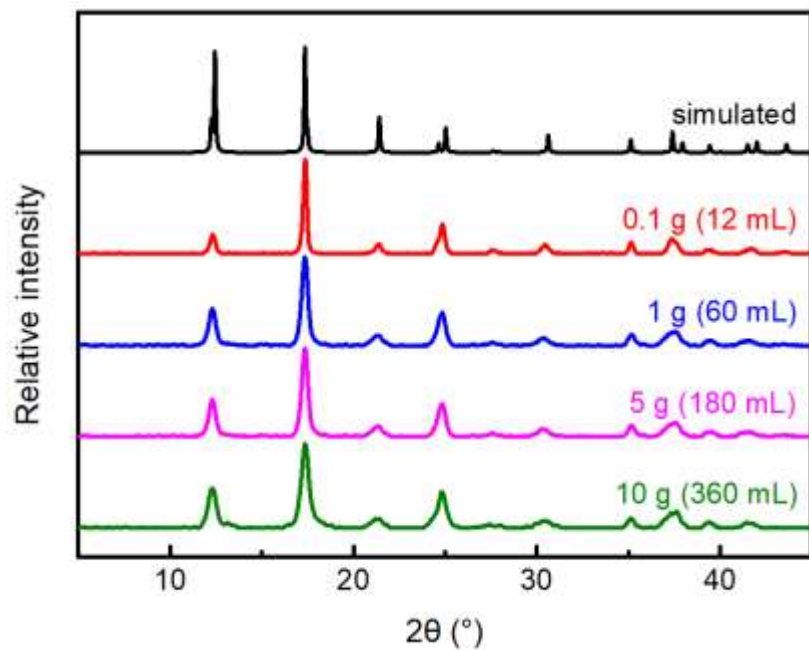


Figure S37. PXRD patterns of ZJU-74 bulk samples from different vessels, revealing the excellent scalability of ZJU-74 that can be easily obtained up to multigram yield.

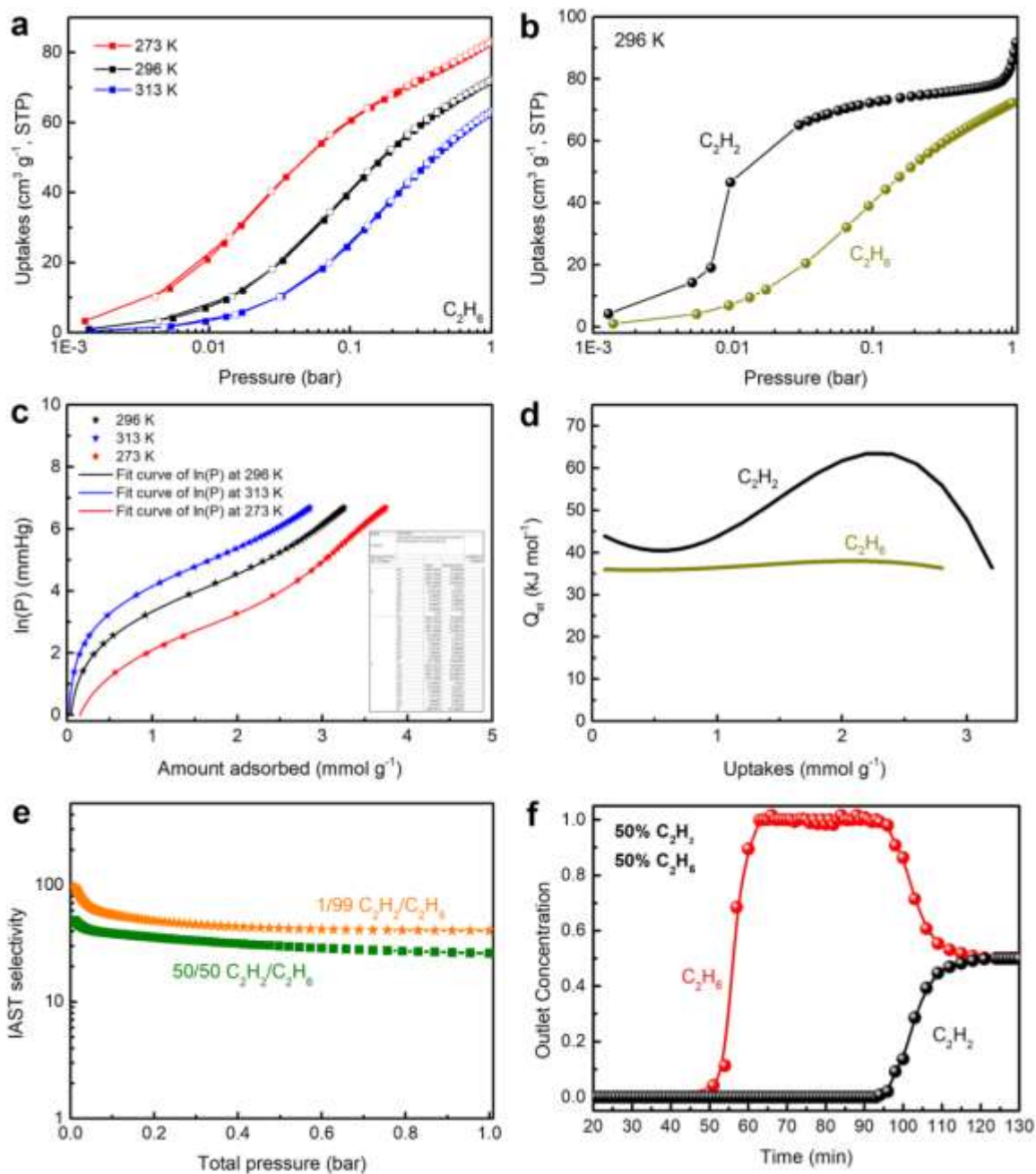


Figure S38. a) C_2H_6 adsorption isotherms of ZJU-74a at 273 (red), 296 (black) and 313 K (blue). Filled/empty symbols represent adsorption/desorption. b) Gas adsorption isotherms of ZJU-74a for C_2H_2 (black) and C_2H_6 (yellow) at 296 K. c) Virial fitting of the C_2H_6 adsorption isotherms for ZJU-74a. d) Heats of adsorption (Q_{st}) of C_2H_2 (black) and C_2H_6 (yellow) for ZJU-74a. e) IAST selectivities of ZJU-74a for C_2H_2/C_2H_6 mixtures at 296 K. f) Experimental column breakthrough curves for a 50/50 C_2H_2/C_2H_6 mixture with a total flow of 2 mL min^{-1} in an absorber bed packed with ZJU-74a at 298 K and 1 bar.

REFERENCES

- [1] R. Krishna, *Microporous Mesoporous Mater.* **2014**, *185*, 30.
- [2] R. Krishna, *RSC Adv.* **2015**, *5*, 52269.
- [3] R. Krishna, *RSC Adv.* **2017**, *7*, 35724.
- [4] R. Krishna, *Sep. Purif. Technol.* **2018**, *194*, 281.
- [5] Y.-L. Peng, T. Pham, P. Li, T. Wang, Y. Chen, K.-J. Chen, K. A. Forrest, B. Space, P. Cheng, M. J. Zaworotko, Z. Zhang, *Angew. Chem., Int. Ed.* **2018**, *57*, 10971.
- [6] P. Li, Y. He, Y. Zhao, L. Weng, H. Wang, R. Krishna, H. Wu, W. Zhou, M. O’Keeffe, Y. Han, B. Chen, *Angew. Chem., Int. Ed.* **2015**, *54*, 574.
- [7] H. S. Scott, M. Shivanna, A. Bajpai, D. G. Madden, K.-J. Chen, T. Pham, K. A. Forrest, A. Hogan, B. Space, J. J. Perry IV, M. J. Zaworotko, *ACS Appl. Mater. Interfaces* **2017**, *9*, 33395.
- [8] J. Lee, C. Y. Chuah, J. Kim, Y. Kim, N. Ko, Y. Seo, K. Kim, T. H. Bae, E. Lee, *Angew. Chem., Int. Ed.* **2018**, *57*, 7869.
- [9] F. Luo, C. S. Yan, L. L. Dang, R. Krishna, W. Zhou, H. Wu, X. L. Dong, Y. Han, T.-L. Hu, M. O’Keeffe, L. L. Wang, M. B. Luo, R.-B. Lin, B. Chen, *J. Am. Chem. Soc.* **2016**, *138*, 5678.
- [10] Y.-P. Li, Y. Wang, Y.-Y. Xue, H.-P. Li, Q.-G. Zhai, S.-N. Li, Y.-C. Jiang, M.-C. Hu, X. Bu, *Angew. Chem., Int. Ed.* **2019**, *58*, 13590.
- [11] K.-J. Chen, H. S. Scott, D. G. Madden, T. Pham, A. Kumar, A. Bajpai, M. Lusi, K. A. Forrest, B. Space, J. J. Perry IV, M. J. Zaworotko, *Chem* **2016**, *1*, 753.
- [12] Y. Ye, Z. Ma, R.-B. Lin, R. Krishna, W. Zhou, Q. Lin, Z. Zhang, S. Xiang, B. Chen, *J. Am. Chem. Soc.* **2019**, *141*, 4130.
- [13] H. Zeng, M. Xie, Y.-L. Huang, Y. Zhao, X.-J. Xie, J.-P. Bai, M.-Y. Wan, R. Krishna, W. Lu, D. Li, *Angew. Chem., Int. Ed.* **2019**, *58*, 8515.
- [14] S. Xiang, W. Zhou, Z. Zhang, M. A. Green, Y. Liu, B. Chen, *Angew. Chem., Int. Ed.* **2010**, *49*, 4615.
- [15] B. Li, X. Cui, D. O’Nolan, H.-M. Wen, M. Jiang, R. Krishna, H. Wu, R.-B. Lin, Y.-S. Chen, D. Yuan, H. Xing, W. Zhou, Q. Ren, G. Qian, M. J. Zaworotko, B. Chen, *Adv. Mater.* **2017**, *29*, 1704210.
- [16] M. J. Katz, Z. J. Brown, Y. J. Colón, P. W. Siu, K. A. Scheidt, R. Q. Snurr, J. T. Hupp, O. K. Farha, *Chem. Commun.* **2013**, *49*, 9449.
- [17] Y. Pan, Y. Liu, G. Zeng, L. Zhao, Z. Lai, *Chem. Commun.* **2011**, *47*, 2071.

[18] J. An, S. J. Geib, N. L. Rosi, *J. Am. Chem. Soc.* **2009**, *131*, 8376.

[19] R.-B. Lin, L. Li, H. Wu, H. Arman, B. Li, R.-G. Lin, W. Zhou, B. Chen, *J. Am. Chem. Soc.* **2017**, *139*, 8022.